Barents Sea plankton production and controlling factors in a fluctuating climate

Anne Britt Sandø [iD] [1,2]*, Erik Askov Mousing[1,2], W. P. Budgell[1,2], Solfrid S. Hjøllo[1,2], Morten D. Skogen[1,2], and B. Ådlandsvik[1,2]

[1]*Oceanography and climate, Institute ofMarine Research, Bergen, Pb.1870, N-5817, Norway*
[2]*Bjerknes Centre for Climate Research, Bergen, Pb. 7803, N-5020, Norway*

Corresponding author: tel: +47 934 34 060; e-mail: anne.britt.sando@imr.no.

The Barents Sea and its marine ecosystem is exposed to many different processes related to the seasonal light variability, formation and melting of sea-ice, wind-induced mixing, and exchange of heat and nutrients with neighbouring ocean regions. A global model for the RCP4.5 scenario was downscaled, evaluated, and combined with a biophysical model to study how future variability and trends in temperature, sea-ice concentration, light, and wind-induced mixing potentially affect the lower trophic levels in the Barents Sea marine ecosystem. During the integration period (2010–2070), only a modest change in climate variables and biological production was found, compared to the inter-annual and decadal variability. The most prominent change was projected for the mid-2040s with a sudden decrease in biological production, largely controlled by covarying changes in heat inflow, wind, and sea-ice extent. The northernmost parts exhibited increased access to light during the productive season due to decreased sea-ice extent, leading to increased primary and secondary production in periods of low sea-ice concentrations. In the southern parts, variable access to nutrients as a function of wind-induced mixing and mixed layer depth were found to be the most dominating factors controlling variability in primary and secondary production.

Keywords: Barents Sea, gross primary production, gross secondary production, NorESM1-M, NORWECOM.E2E, photosynthetic available radiance, RCP4.5, ROMS, temperature, wind-induced mixing

Introduction

The Barents Sea (BS) is the largest and deepest of the continental shelf seas surrounding the Arctic Ocean. It is a transition zone for warm and saline water moving from the Atlantic to the Arctic Ocean, as well as for cold and less saline water en route from the Arctic to the Atlantic. The inflow of warm and saline water into the BS, and fluxes between the ocean and atmosphere therein, are of significant importance to the regional climate and biomass production. More specifically, the spring bloom is one of the most characteristic features in ocean productivity at high latitudes, responding to seasonal increases in irradiance and stratification (e.g. Yool *et al.*, 2015; Lee *et al.*, 2016) and makes the BS an important site for commercial fisheries through bottom-up

processes (Johannesen *et al.*, 2012). For several years, surface air temperatures in the Arctic have increased at twice the global rate (Hansen *et al.*, 2006; Skagseth *et al.*, 2015), where the spatially averaged warming north of 60°N has been 1–2°C since the temperature minimum in the 1960s and 1970s (IPCC, 2013). Both air and ocean temperatures show strong multi-decadal variability on timescales of 50–80 years (Zhang *et al.*, 2007), and this large-amplitude multi-decadal climate variability impacting the Arctic may cause confusion in the detection of the true underlying climate trend over the past century (Polyakov *et al.*, 2003). Furthermore, variability in terms of atmospheric forcing and propagation of hydrodynamic anomalies in the ocean may also work on different temporal and spatial scales.

It is therefore important to bear in mind these effects of natural variability and the timescales they are working on when analysing model results addressing climate change and its impacts on marine ecosystems, especially when the spatial scale decreases from the global to the regional scale (Bopp *et al.*, 2013; Frölicher *et al.*, 2016).

A growing number of studies indicate major changes to marine systems, including increased ocean temperature (Rahmstorf *et al.*, 2007; Cheng *et al.*, 2017), increased acidification (Orr *et al.*, 2005), and changes in ocean currents (Böning *et al.*, 2008; Liu *et al.*, 2017), leading to ocean conditions not seen for hundreds of thousands of years (Hoegh-Guldberg and Bruno, 2010). These effects have major impacts on marine ecosystems, including changes in total productivity and ecosystem structure (Behrenfeld *et al.*, 2006; Arrigo *et al.*, 2008; Fossheim *et al.*, 2015; Yool *et al.*, 2015; Barton *et al.*, 2016; Jensen *et al.*, 2017).

While the effects of climate change are evident in most of the world's oceans, they are of particular interest in the Arctic due to the amplified temperature increase resulting in a fundamental change from a seasonally ice-covered to a permanently open ocean system in the BS (Arrigo *et al.*, 2008; Stroeve *et al.*, 2012; Screen and Williamson, 2017). The northern and eastern parts of the BS are currently seasonally ice-covered, and a large proportion of the yearly primary production is coupled to the phytoplankton bloom happening when the sea-ice retreats in the spring (Wassmann *et al.*, 1999). A future ice-free BS resulting from warming will likely lead to significant changes in spring bloom dynamics, total productivity, and ecosystem structure. Ecosystem changes would, in part, be due to changes in the food availability to higher trophic levels (Kahru *et al.*, 2011; Arrigo *et al.*, 2008) as well as the movement of boreal species towards higher latitudes (Perry *et al.*, 2005; Fossheim *et al.*, 2015; Barton *et al.*, 2016; Jensen *et al.*, 2017). Temperature itself fundamentally affects all biological and ecological processes (Brown *et al.*, 2004), which would affect not only the primary producers but all trophic levels in the entire BS (Fossheim *et al.*, 2015). In addition to heat, the Norwegian Atlantic Slope Current and the Norwegian Coastal Current transport vast numbers of organisms into the BS and the abundance of *Calanus finmarchicus* in the BS thus depends on inflow from the Norwegian Sea (Skaret *et al.*, 2014).

Most studies on interactions between climate fluctuations and effects on the marine ecosystems are based on analyses of observations from recent decades and corresponding climate conditions. A relevant question is therefore if today's knowledge about species' temperature tolerance and effects of temperature fluctuations can be applied to the future under continued global warming? In a comparison of 11 earth system models investigating future primary productivity in the Arctic Ocean, the model mean predicted a general increase in productivity, but individual models differed in the sign of future productivity changes (Vancoppenolle *et al.*, 2013). Based on a comparison of five coupled biological ocean models from the Arctic Ocean Intercomparison Project, Popova *et al.* (2012) emphasized the importance of a realistic representation of ocean physics, in particular vertical mixing, as a necessary foundation for ecosystem modelling and predictions. They also found that the main source of uncertainty is related to the sea-ice zones, highlighting the need for downscaled and more accurate regional implementations of the physical forcing.

Unfortunately, global climate models with the high horizontal resolution are computationally expensive to run and most current global models do not have sufficient resolution to properly resolve the relevant circulation features and constraints such as bottom topography in the BS (Sandø *et al.*, 2014b; Skogen *et al.*, 2018). Downscaling with regional models is therefore needed to improve issues of northward heat transport, sea-ice extent, and regional distribution in the BS.

The objective of this study is to combine results from a downscaled climate model and an ecosystem model to investigate how changes in radiative forcing in a moderate emission scenario (RCP4.5) lead to changes in environmental factors such as temperature, sea-ice concentration, stratification, and wind-generated vertical mixing, and how these changes lead to changes in primary and secondary production. We hypothesize that (i) the heat transport into the BS through the BS Opening (BSO) is important for the variability of the primary and secondary production in the BS in terms of light as a function of sea-ice concentration and vertical mixing of nutrients as a function of stratification; and (ii) The primary and secondary production will increase in the BS due to future warming.

Methods

To study the future effects of climate change on primary and secondary production in the BS, physical variables such as velocity components, temperature, salinity, sea surface height, and sea-ice concentration from a downscaled climate model projection together with wind components and shortwave radiation from a global model projection were used as input to an ecosystem model. Thereafter, statistical models were used to study the relationships between the physical forcing and the biological production on seasonal and decadal timescales.

Global climate model

The Coupled Model Intercomparison Project Phase 5 (CMIP5) offers many global climate models that can be used in downscaling, but one must be aware that every model has strengths and weaknesses. Although the latest IPCC report (AR5 IPCC, 2013) confirms the results from the previous IPCC report (AR3 IPCC, 2007) about projected strong decreases in sea-ice concentration in the Arctic towards the end of this century, the inter-model spread is considerable (IPCC, 2013). It is therefore crucial, before conducting downscaling, to evaluate the different climate models for agreement with the observed values of the most relevant variables in the region of interest, both with respect to mean and variability. To get an estimate of the uncertainty in the results, it is also desirable to downscale an ensemble of models, but time and computational resources often put constraints on this.

For this study, where heat content and sea-ice concentration is of importance to the regional ecosystem, evaluation of the heat transport into the BS and Arctic is of particular importance. Ocean heat transport through different sections into the BS and Arctic Ocean, and its impacts on sea-ice processes and variability were the focus in a study prior to this (Sandø *et al.*, 2014a). Three coupled climate models (CNRM-CM5, MRI-CGCM3, and NorESM1-M) were evaluated against multiple estimates from the literature with respect to poleward heat transport through four gateways to the Arctic. It was concluded that NorESM1-M transports were closest to the mean in both the BSO and the Fram Strait. These are the gateways that are closest to the region of interest in this study, and NorESM1-M was therefore chosen for downscaling in this analysis.

The future climate is strongly dependent on future emissions of greenhouse gasses. Four different representative concentration pathways (RCPs) are used to describe a set of greenhouse gas concentration trajectories adopted by the IPCC for its fifth Assessment Report (AR5) in 2013. These are RCP2.6, RCP4.5, RCP6, and RCP8.5. Of these, the RCP4.5, in which the emissions peak around 2040, decline, resulting in a stabilization of the radiative forcing of $4.5 \, \text{W m}^{-2}$ relative to preindustrial time, is used for downscaling in this study. In addition to uncertainty due to model errors and internal variability in the climate system, the choice of RCP scenario descriptions is one of the main uncertainty components in the surface temperature projections (Hawkins and Sutton, 2009). A reasonable start would be to downscale one scenario in the middle of the four scenarios in addition to two extremes, but as in selecting global models for downscaling, our limitations of computational time made it necessary to choose one. RCP4.5 is chosen as it represents something between the extremes and as it is also commonly used in other impact and downscaling studies (Knutson *et al.*, 2015; Hermans *et al.*, 2020).

Regional ocean model

Downscaling was done using the Regional Ocean Model System (ROMS) (Shchepetkin and McWilliams, 2005). Previous applications of the model in the Nordic and Barents Seas are described in Budgell (2005), Ådlandsvik and Bentsen (2007), Ådlandsvik (2008), Lien *et al.* (2013, 2014), Lien and Ådlandsvik (2014), and Lien *et al.* (2016). The regional model set-up was initialized from the NorESM1-M model (Bentsen *et al.*, 2013), and results from this model were also used at the open boundaries and as atmospheric forcing. A weak relaxation with a time scale of 360 days towards NorESM1-M sea surface salinity was also applied. The model was run on a stretched orthogonal curvilinear grid with an average resolution of 10 km in the BS and is covering the Arctic and the Atlantic Ocean to about 20°S. There are 40 generalized sigma (s-coordinates) levels in the vertical dimension, applying the scheme of Song and Haidvogel (1994), with stretching that enhances the resolution towards the bottom and the surface. Lateral motions and diffusive energy losses induced by small-scale processes are related to the gradients of the mean velocities and tracers by eddy viscosity and diffusivity coefficients (Smagorinsky, 1963). For advection, we use the third-order upwind biased scheme proposed by Shchepetkin and McWilliams (2008). ROMS employs split-mode explicit time stepping, and in this study, the baroclinic mode time step was 100 s, while the barotropic mode time step was 10 s. An ice-ocean drag coefficient of 7.5×10^{-3} is applied at the ocean surface. This is a concentration-weighted combination of ice-ocean stress and air-sea stress, where at zero ice cover, there is zero contribution from ice-ocean stress. As summarized by Lu *et al.* (2011), the value of 7.5×10^{-3} for this coefficient is a typical value for ice floes of moderate roughness in marginal ice zones such as in the Bering Sea and Greenland Sea. They also find a relationship between ice concentration and the ice-ocean drag coefficient which is non-monotonic (Lu *et al.*, 2011), but this requires knowledge of variables such as ice floe size distribution which is not available in our study.

The model has previously been used to downscale two global climate models from CMIP3 on exactly the same area for the 20C3M control run and the A1B scenario and has been thoroughly evaluated (Sandø *et al.*, 2014b). In that study, the two global models GISS AOM and NCAR CCSM3 were downscaled to investigate how a regional model should be set up to take advantage of the results from the global projections. For the historical simulations, the downscaled results were closer to observations than the global model results they were downscaled from. The improvements were due to more detailed topography and realistic circulation and inflow of warm Atlantic Water through the BSO. Realistic inflow of Atlantic Water with respect to volume and heat is shown to be of great importance for the variability of the sea-ice concentration in the region (Sandø *et al.*, 2010; Årthun *et al.*, 2012; Sandø *et al.*, 2014a,b; Onarheim *et al.*, 2015). Despite the improvements gained by downscaling of the historical simulations, salinity biases of opposite signs in the two global models' future projections made it impossible to draw any conclusions about the future freshwater distributions in the BS (Sandø *et al.*, 2014b).

The effects of using different global and regional models were studied in Schrum *et al.* (2015), who concluded that regional downscalings of one global model using different regional models gave minor differences, while using only one regional model with forcing from different global models resulted in more pronounced divergence. These results on model uncertainty due to biases or diverging results in global climate models are important to keep in mind when analysing downscaled climate projections. Moreover, based on experience from the ENSEMBLES project (http://ensembles-eu.metoffice.com), it was recommended to use results based on two or more regional climate models that again are forced by at least two global climate models for climate impact studies. A comparison between the regional ROMS model used here and the global NorESM1-M that it was downscaled from was performed by Skogen *et al.* (2018). They concluded that the global and regional model compared well on trends, but that details were lost when the coarse resolution global model was used to assess climate impact on regional scale. The main difference between the two models was the timing of the spring bloom, and a non-exhaustive nutrient consumption in the global model in summer.

To evaluate ROMS results directly against observed time series from recent decades, a hindcast simulation forced with CORE2 reanalysis from 1958 to 2007 (Large and Yeager, 2009) was performed. Thereafter, the same regional model was used to downscale the future scenario RCP4.5 from the global NorESM1-M for the period 2006–2070. The data to evaluate the models were downloaded from the NMDC (https://www.hi.no/hi/forskning/prosjekter/norwegian-marine-data-centre-nmdc) and AtlantOS (http://www.oceansites.org/tma/index.html). The observations were detrended and presented exactly the same way as the modelled transports, and they are fully independent of the model.

Ecosystem model

To investigate how climate change affects the lower trophic levels in the BS ecosystem, the physics from the NorESM1-M RCP4.5 scenario downscaled with ROMS were used to force the NORWegian ECOlogical Model system End-To-End (NORWECOM.E2E) (Aksnes *et al.*, 1995; Skogen *et al.*, 1995; Skogen and Søiland, 1998). This model is a coupled physical-biogeochemical model system developed to study primary production, nutrient budgets, and dispersion of particles such as fish larvae and pollution and has been validated by comparison with field data in the Nordic and Barents Seas (Skogen *et al.*, 2007;
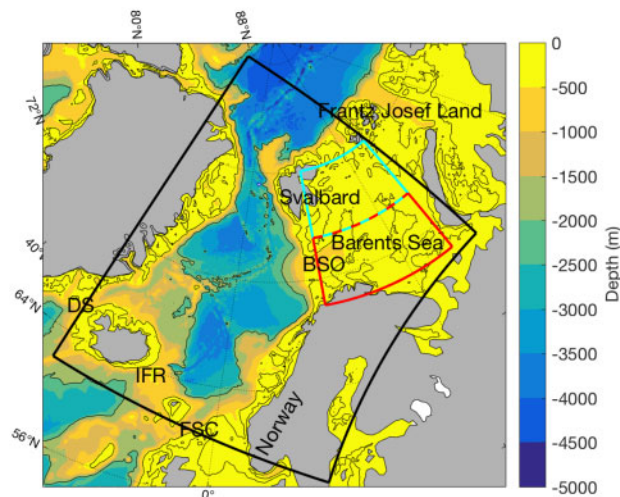
Figure 1. Model domain of the biophysical model (black outline). The analysis of the Barents Sea is divided into a southern (red) and a northern (blue) part with dashed lines. Sections used for evaluation are Denmark Strait (DS), Iceland-Faroe Ridge (IFR), Faroe-Shetland Channel (FSC) and Barents Sea Opening (BSO).

Hjøllo et al., 2012; Skaret et al., 2014). The prognostic variables are dissolved inorganic nitrogen, phosphorous, silicate, two different types of phytoplankton, two detritus pools, diatom skeletal, silica, oxygen, and two types of zooplankton. Equations and further model details are given in the Appendix.

In the present study, the model was run in offline mode using 5-day means of the physical ocean fields (velocities, salinity, temperature, sea surface height, and sea-ice) from the ROMS downscaling together with atmospheric fields from the NorESM1-M (wind and short wave radiation that is linearly reduced by multiplication with (1-c)). The horizontal grid used (Figure 1) was identical to a subdomain of the original ROMS grid, and the time step was 3600 s.

Initial fields for nutrients were interpolated from annual means of the NorESM1-M simulation for the years 2001–2005, except for silicate that has a large offset in the NorESM1-M simulation with surface values close to 20 µM in the area of interest caused by advection of water with high silicate from the Bering Sea. For silicate, typical winter values of Atlantic Water in the Norwegian Sea (5.5 µM, Fransico Rey, pers.comm.) were therefore used. Initial concentrations of 0.10 mgN m^{-3} for phytoplankton were used for both diatoms and flagellates. These values were also used at the open boundaries. Inorganic nitrogen is added to the system from the atmosphere, while there is no river input of nutrients. To absorb inconsistencies between the forced boundary conditions and the model results, a 7-grid cell "Flow Relaxation Scheme" zone (Martinsen and Engedahl, 1987) was used around the open boundaries. The simulation started on 1 January 2006. After a 12 year spin-up (running the first year 12 times), the full model period (2006–2070) was run sequentially.

Data preparation and statistical methods

Statistical analyses were performed using the free and open-source statistical software R version 3.4.2 (R Core Team, 2019). Biological variables extracted from the NORWECOM.E2E model was depth-integrated gross primary production (GPP), and gross secondary production (GSP). Physical variables were extracted

from the ROMS and NorESM1-M models and included sea surface temperature, sea-ice concentration as well as surface wind velocity and stress. In order to determine the relationship between productivity and the environmental variables, data were only extracted from the productive months (April to September). In addition, the data were split into southern and northern parts of the BS (Figure 1) and analysed individually for each region. Due to strong salinity biases in the global model (NorESM1-M) (Skogen et al., 2018), the regional model used a weak relaxation to sea surface salinity. Such corrections would lead to a less realistic evolution in the sea surface salinity. Temperature was therefore chosen as the criterion in the mixed layer depth (MLD) definition to give a more realistic picture of the trend and variability, which is a central part of this study. The MLD was determined as the depth at which the temperature difference compared to the surface was equal to a defined threshold value of 0.5°C. Although sea-ice freezing and melting would tend to change the stratification and the mixed layer depth, it is not explicitly studied here. Wind-induced mixed layer turbulent energy production (u^{*3}) was calculated following Klinger et al. (2006). Spring bloom initiation day (BID) was determined as the day the daily production exceeded a threshold value of 5% above the yearly median production (Brody et al., 2013). Low winter values were excluded for the calculation of the median by removing days with daily production lower the 0.01 g m^{-2} day^{-1}.

Simple bivariate relationships were assessed using Pearson product-moment correlation coefficients. Multivariate relationships between primary production and the environment were assessed with general linear regression models using ordinary least square estimation. Explanatory variables were temperature, wind-induced mixed layer turbulent energy, and photosynthetically active radiation (PAR), hereafter referred to as light. All variables were standardized (0 mean and standard deviation of 1), and the resulting coefficients were thus beta-coefficients, suitability for comparing the relative importance of each independent variables. Temporal autocorrelation was investigated using two different approaches. First, two model candidates were constructed with all the explanatory variables but with one model including an autocorrelation structure of order 1 (corAR1; Box et al., 2015). These two models were then compared using the Akaike Information criterium (AIC; Burnham and Anderson, 2002). AIC identified the model without an autocorrelation structure as the most parsimonious model. In addition, the models were assessed visually by plotting the autocovariance which identified no significant autocorrelation. Thus, the model excluding an autocorrelation structure was chosen. Model assumptions of multivariate normality, collinearity, and homoscedasticity were assessed visually (i.e. investigation of the residual patterns vs. fitted values and theoretical quantiles), and by calculating the variance inflation factors (i.e. VIF scores).

Mean values and mean change of all variables were calculated for the production months in the periods 2010–2019 and 2060–2069 as well as the periods 2028–2044 and 2046–2052 between which environmental and biological variables showed particularly abrupt change.

Results

Change in physical conditions and biological production in the downscaled RCP4.5 scenario (2010–2070)

To justify the use of the regional model for future projections of BS climate, the model was evaluated with respect to Atlantic

Water transports through different sections, (Supplementary Figure S1), the Marginal Ice Zone (MIZ) variability (Supplementary Figure S2), and how downscaling improves the sea-ice concentration (Supplementary Figure S3). Considering the uncertainties in the observed and simulated time series, the evaluation showed that the model reproduced the mean of the transports, the MIZ index, and their corresponding variability in an acceptable way. This is further presented and discussed in the Supplementary material.

Results from the last decade of the downscaled simulation, 2060–2069, hereafter called the future decade, are compared to the first decade of the same simulation, 2010–2019, hereafter called the present decade. The choice of the two decades to illustrate the future change may therefore be strongly influenced by the natural variability, but the time series shown in Figure 2 reveals that the decades chosen (2010s and 2060s) represent anomalies of the same sign relative to the trend (dashed line), and will therefore not represent a change that is strengthened by natural variability. Figure 3a shows the path of the relatively warm Atlantic Water off the northern coast of Norway and how it splits into two branches, wherein one continues towards the western coast of Svalbard as the West Spitsbergen Current, and the other into the BS. Likewise, the depth-integrated map of annual mean GPP in Figure 4a reveals a pattern of high production in the fresh Norwegian Coastal Current and in the MIZ (low sea-ice concentration) area south of Svalbard (Figure 3c). Conversely, reduced levels of GPP were associated with relatively cold areas with high sea-ice concentration. Area-averaged GPP per season (April to September) was ~153 and 141 gC m^{-2} season^{-1} for the southern and northern BS, respectively. The change in yearly mean temperature between the two decades 2010–2019 and 2060–2069 is shown in Figure 3b. The projected change in the BS was about 0.5–1°C in most parts, slightly higher southeast of Svalbard and in the eastern parts of the BS. This is also partly reflected in the loss of sea-ice in these regions as shown in Figure 3d.

The GPP difference between the present and future decade during the season from April to September is shown in Figure 4b. The future change shows a slight increase in GPP in the northern BS and in the BSO as well as along the Norwegian coast. In the central BS, some areas with a decrease in GPP production are found, but generally, the changes were smaller here. Area-averaged GPP values for the future decade increased to ~156 and 145 gC m^{-2} season^{-1} for the southern and northern BS, respectively (Table 1), resulting in only a small increase in GPP of ~3 and 4 gC m^{-2} season^{-1} (or 2.1% and 3.0%), respectively.

Gross secondary production (GSP) for the present decade of the simulation (Figure 4c) was highest in the southwestern parts, decreasing northwards and eastwards. Mean GSP over the period was 63 and 50 gC m^{-2} season^{-1} in the southern and northern BS, respectively. Similar to the pattern for GPP, there was a slight increase in GSP in the BS inflow area as well as in the northern part of the BS. However, in most of the BS, there was no clear change in the GSP between the present and future decade (Figure 4d). GSP in the future decade corresponded to area-averaged values of ~66 and 53 gC m^{-2} season^{-1} for the southern and northern BS, respectively. That is, the simulation showed only a small increase in GSP of ~3 gC m^{-2} season^{-1} for both regions, or 3.8% and 4.8% in the southern and northern regions, respectively. Thus, GPP and GSP were higher in the southern BS than in the northern, with a mean difference of about 12 and 13 gC m^{-2} season^{-1}, respectively, but in terms of percental change, the northern BS exhibited a slightly larger increase for both GPP and GSP, and the relative increase was larger for GSP compared to GPP (Table 1).

Decadal climate variability and associated responses in biological production

Integrated over the BS southern and northern regions, both GPP and GSP exhibited a large degree of inter-annual variability. The variability in terms of the coefficient of variation (CV) was larger in the north (CV = 0.072 and 0.097 for GPP and GSP, respectively) compared to the south (CV = 0.047 and 0.065, respectively) (Figure 2). In both the southern and northern BS, GPP and GSP showed an increasing trend from 2010 until the mid-2040s. Then, there was a significant drop in GPP and GSP after which they both recovered towards the end of the simulation at approximately the same rate as the pre-2040s period. This drop in the mid-2040s was most pronounced in the northern BS, but the pattern was also present in the south. Overall, there was only a very small increase in GPP during the course of the simulation with the north exhibiting a slightly larger increase (Table 1) compared to the south. The vertical dashed lines in Figure 2 indicate the beginning and the end of a warm (W) and a cold (C) anomaly before and after the mid-2040s, respectively, and mean values of biological and environmental variables and associated changes between warm (2028–2044) and the cold (2046–2052) periods are shown in (Table 2). Furthermore, Figure 2 suggests that the inflow of Atlantic Water through the BSO affected the temperature and nitrate content in the BS, especially in the southern part. Similarly, the figure indicates that heat transport influenced the sea-ice concentration, and thereby also light availability, in the northern part.

The southern BS MLD showed a general decrease in the period, consistent with a general temperature increase. There were no prominent differences between the north and the south, with the exception of the period from the mid-2040s to the beginning of the 2050s where mixed layer depth decreased in the north and increased in the south. Wind-induced mixing showed similar inter-annual variability for both the southern and northern BS, but with generally lower values in the north compared to the south.

Seasonally averaged light showed significant inter-annual variation, but no overall trend was identified during the simulation period in either region. In the north, the inter-annual variation was significantly negatively correlated with sea-ice extent ($r = -0.49; p < 0.001$) which is most clear in the mid-2040s where light availability abruptly decreased, concomitantly with the increase in sea-ice extent. In the southern BS however, sea-ice extent exhibited only minor changes.

To further analyse the effect of temperature, sea-ice concentration, wind-induced mixed layer turbulent energy production, and light on GPP, multiple linear regression models were used. Due to the correlation between temperature and sea-ice concentration, only temperature was included in Table 3. The overall fit of the models were $R^2 = 0.34$ and $R^2 = 0.62$ for the southern and northern BS, respectively. Based on the yearly means, the models showed all three variables to have strong effects on GPP with an increase in variables to be associated with an increase in GPP. However, based on the correlation coefficients, the relative
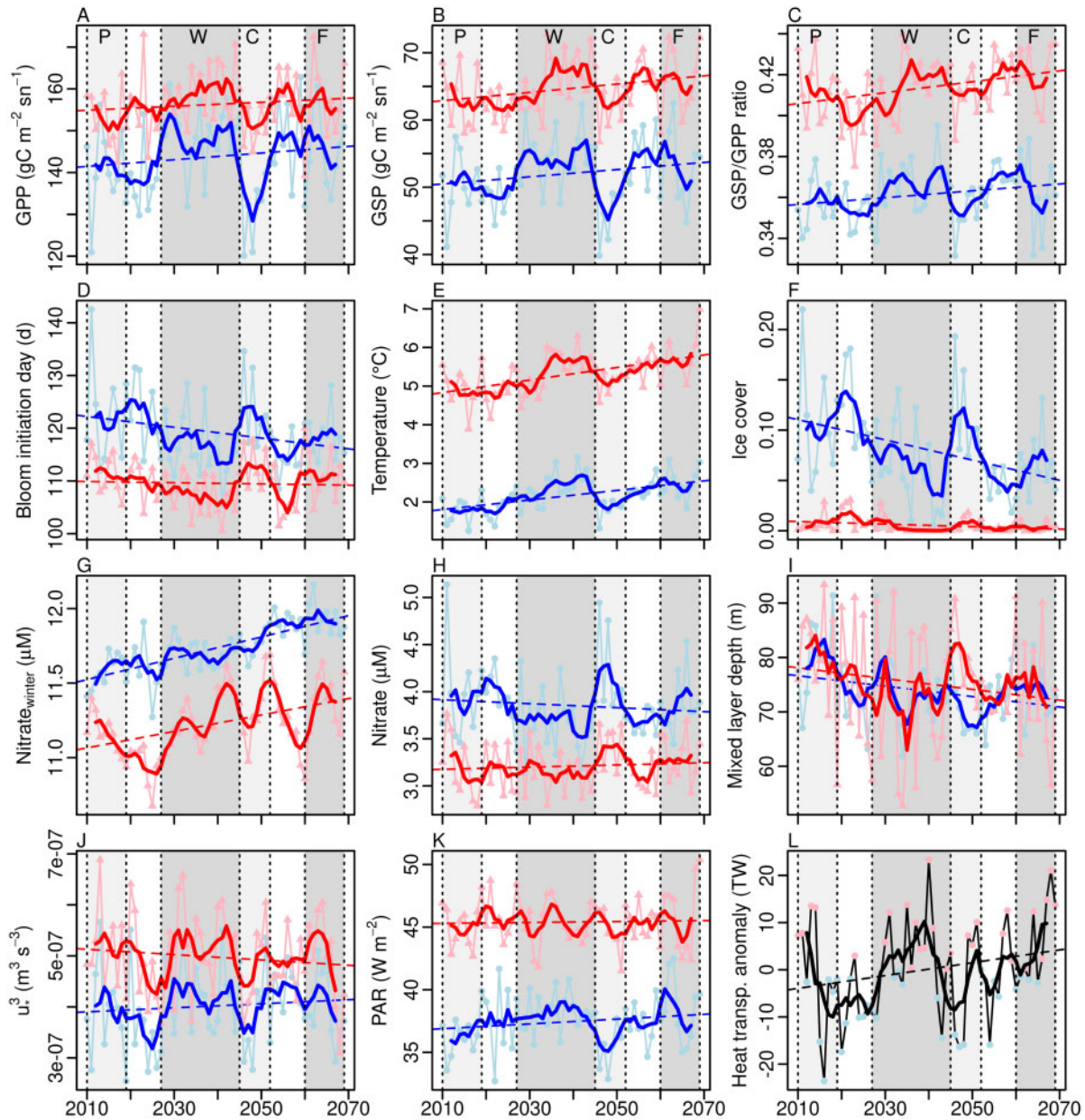
Figure 2. Time series of northern (blue) and southern (red) Barents Sea gross primary production (GPP), gross secondary production (GSP), GSP/GPP, bloom initiation day, temperature, ice cover, pre-bloom nitrate (Nitrate$_{winter}$), nitrate during production months (Nitrate), mixed layer depth, wind-induced mixed layer turbulent energy production (u^{*3}), light in terms of photosynthetic available radiance (PAR), and heat transport anomaly in BSO. All time series show the production months (April to September), except pre-bloom nitrate which is from January to March. All values are surface values, except the vertically integrated, GPP, GSP, and heat transport anomaly. P, F, W, and C denote present, future, warm, and cold periods, respectively, and thick lines 5 year running means.

importance of the variables differed between regions. Thus, in the southern BS, GPP was more strongly associated with mixed layer turbulence compared to temperature and light availability whereas in the northern BS, GPP was more strongly associated with light availability compared to temperature and mixed layer turbulence.

Seasonal variability in GPP and GSP

The mean BS spring BID for the present-day climate and its change in the future is shown in Figure 5. For the present-day

climate, spring BID exhibited a latitudinal gradient with the bloom starting earlier in the south and proliferating towards the north. The area with the latest BID day was east of Svalbard in the northernmost parts of the BS where the highest concentrations of sea-ice are found in spring. In the future, spring BID did not show a consistent pattern of change in the southern BS. The major change was found in the northernmost parts, with changes in BID up to 36 days earlier than at present, corresponding to the area exhibiting the largest decrease in sea-ice concentration (Figure 3). Averaged across the regions, spring BID from the
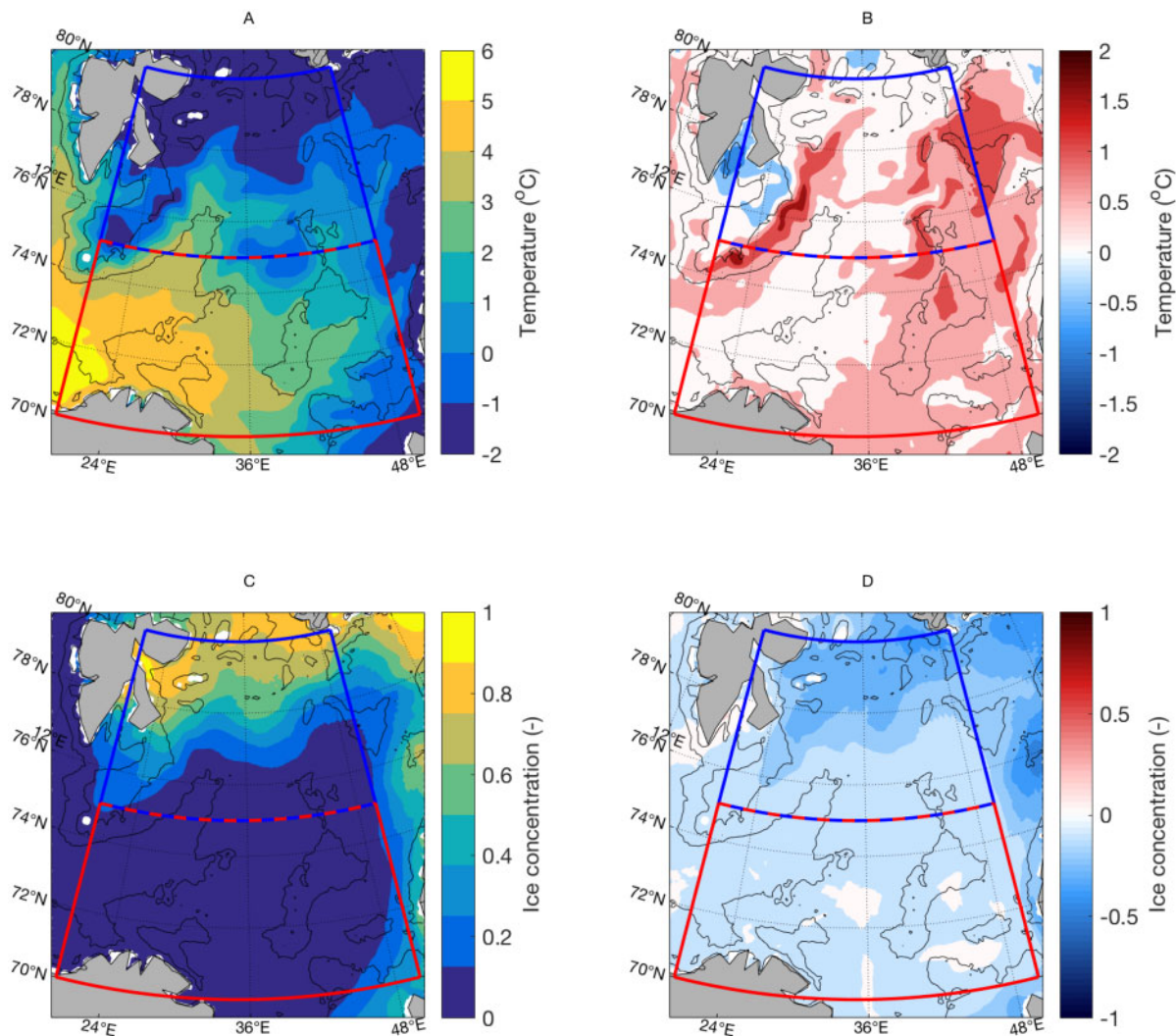
Figure 3. Decadal mean ROMS spring sea surface temperature (°C) for the present decade (2010–2019) (a) and corresponding change between the present and future decade (2010–2019 to 2060–2069) (b), fraction of sea-ice (-) (c) and corresponding change (d). Spring is the mean of March and April. The Barents Sea is divided into a southern (red lines) and northern (blue lines), and bathymetry is indicated by thin black contour lines at 300 m and 2000 m.

present to the future changed 0.2 and −4.1 days in the southern and northern BS, respectively (Table 1).

The seasonal variations in the primary and secondary production along with the different physical variables of interest in the present and future decade of simulation are shown in Figure 6. The onset of an increase in GPP and GSP during the present decade was in April and May, respectively, with corresponding maxima 2 months later. Increasing GPP was associated with increasing light availability and decreasing MLD and nitrate concentrations in both regions. In the northern BS, increases in light availability also followed decreases in sea-ice concentration.

In general, there were only minor changes in the seasonal dynamics in the future compared to the present climate. In the southern BS, the majority of variables were essentially the same, with the exception of temperature. In the northern BS, sea-ice concentration showed relatively large decreases in the future but the overall dynamics were similar. However, with the overall lower sea-ice concentration, the future seasonal dynamics also showed increasing wind-induced mixed layer turbulent energy

production during the winter and spring months, a faster increase in light and a faster increase in the evolution of GPP. Thus, in the northern BS, the maximum GPP was moved forward in time from June to May, exhibiting seasonal dynamics more similar to the southern BS.

The relative contribution to GPP and GSP by diatoms and meso-zooplankton, respectively, is illustrated by the dashed lines in Figure 6. These relative contributions to the phyto- and zooplankton communities were inversely proportional to the seasonal evolution of the GPP and GSP themselves, with maxima in the beginning of the spring bloom in April. Thus, at the onset of the spring bloom in April diatoms dominate the production, followed by a mixed community in May and a shift to a flagellate-dominated community from June to September. For the zooplankton, the pattern is similar with mesozooplankton having a high relative contribution to total GSP, followed by a microzooplankton-dominated community for the rest of the productive season. The changes from the present to the future decade are only minor. Seasonal evolution for the warm and cold periods is
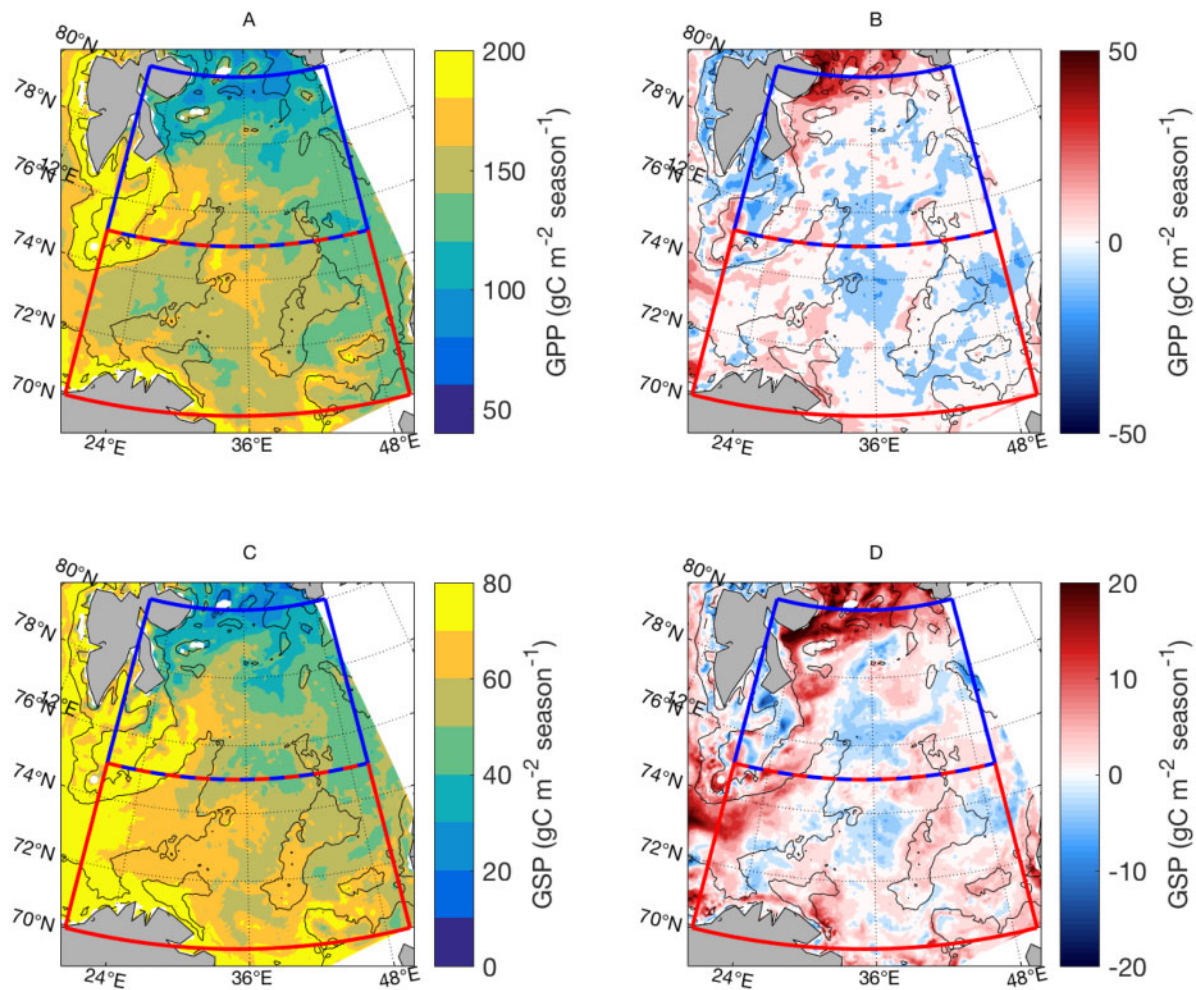
Figure 4. As in Figure 3, but for mean NORWECOM GPP (gC m^{-2} season^{-1}) (a), corresponding change (b), GSP (gC m^{-2} season^{-1}) (c), and corresponding change (d). Season represents the cumulative values in April–September. Note that the upper and lower figures have different colour scales.

shown in Figure 7. Here, the patterns were almost identical to the present and future decade, but with opposite changes in relation to time (i.e. the cold period resembles the present decade, and vice versa).

Discussion

Evaluation of the model system

The objective of this study was to apply a regional model to investigate the effects of future variability and trends in different environmental variables on primary and secondary production in the BS. The regional ocean model ROMS was evaluated for the recent decades using observational time series on volume transports and sea-ice extent. The full evaluation and discussion of these physical variables are given in the Supplementary material, but the short story is that mean values were all within the observed estimates and that the variability was satisfactorily reproduced (Supplementary Figures S1–S3).

In accordance with the results from Slagstad et al. (2011), elevated results of GPP were found to be in relatively warm and shallow areas (Figure 4), but high production was also found at the shallow banks south of Svalbard. The values of 153 and 141 gC m^{-2} season^{-1} for the southern and northern BS (period 2010–

2019, Table 1), were found to be higher than estimates of Titov and Orlova (2011) and Slagstad et al. (2011) who give average BS values of 100 gC m^{-2} season^{-1} and 111 gC m^{-2} season^{-1}, respectively. The primary production in the Barents Sea varies a lot between different water masses. Estimates are also very variable. Titov and Orlova (2011) have summarized some of these and concludes with 174 gC m^{-2} in Atlantic and 66 gC m^{-2} in Arctic water. The Atlantic estimate is therefore in agreement with our BS south, while the Arctic is well below our BS north. Estimating primary production is not straight forward and is normally based on very few samples. In the northern BS, the unfriendly conditions make this even more difficult. In addition, the ice has retreated significantly during the recent decades. The estimate given by Titov and Orlova (2011) is from observations, but we also acknowledge it only as an estimate as it is based on few measurements in space and time with unknown representativeness. The reference is therefore merely included to state that our model is of similar order as other estimates.

Long-term changes in the future projection

The future decade in this study (2060–2069), showed that the strongest warming is projected to take place in the northern part

Table 1. Mean values and mean change of biological (gross primary production (GPP), secondary production (GSP) and bloom initiation day (BID)) and environmental variables (temperature (Temp), sea-ice concentration (Sea-ice con), photoactive radiation (PAR), nitrate concentration (Nitr), winter nitrate concentration (Nitr$_{win}$), mixed layer depth (MLD), wind-induced mixed layer turbulent energy (u*^{3}), and heat transport anomaly (HT anom)) during the growth season (sn) which is the production months from April to September for the present and future decades in the southern and northern Barents Sea.

Period	Barents Sea south			Barents Sea north		
	2010–2019	2060–2069	Change	2010–2019	2060–2069	Change
GPP (gC m−2 sn−1)	153.1	156.3	3.2 (2.1%)	140.6	144.8	4.2 (3.0%)
GSP (gC m−2 sn−1)	63.4	65.8	2.4 (3.8%)	50.3	52.7	2.4 (4.8%)
GSP/GPP (-)	0.414	0.421	0.07 (1.7%)	0.357	0.363	0.006 (1.7%)
BID (d)	111.3	111.5	0.2 (0.2%)	122.6	118.5	−4.1 (3.3%)
Temp (°C)	5.0	5.7	0.7 (15.1%)	1.8	2.5	0.7 (36.3%)
Sea-ice con (-)	0.006	0.004	−0.002 (−27.2%)	0.11	0.06	−0.04 (−39.3%)
PAR (W m^{-2})	45.3	45.7	0.5 (1.1%)	36.4	38.3	1.9 (5.2%)
Nitr (μM)	3.2	3.3	0.1 (3.5%)	4.0	3.9	−0.1 (−2.5%)
Nitr$_{win}$ (μM)	11.2	11.4	0.2 (1.7%)	11.6	11.9	0.3 (3.0%)
MLD (m)	79.5	74.0	−5.5 (−6.9%)	79.1	73.8	−5.2 (−6.6%)
u*^{3} (m^{3}s^{-3})	5.1e−7	4.9e−7	−2.0e−8 (−4.4%)	3.9e−7	4.0e−7	1.0e−8 (2.7%)
HT anom (TW)	−0.9	5.4	6.3	−0.9	5.4	6.3

Winter nitrate is from January to March. GPP, GSP, and heat transport (HT) are depth integrated. Other values are surface values.

Table 2. Same as in Table 1, but for the warm (2028–2044) and cold (2046–2052) intermediate periods in the southern and northern Barents Sea.

Period	Barents Sea south			Barents Sea north		
	2028–2044	2046–2052	Change	2028–2044	2046–2052	Change
GPP (gC m^{-2} sn^{-1})	159.6	151.4	−8.2 (−8.1%)	149.1	132.1	−17.0 (−11.4%)
GSP (gC m^{-2} sn^{-1})	66.3	62.0	−4.3 (−6.5%)	54.8	46.7	−8.1 (−14.7%)
GSP/GPP	0.415	0.409	−0.006 (−1.5%)	0.367	0.353	−0.014 (−3.9%)
BID (d)	107.0	112.9	5.9 (5.5%)	116.4	123.2	6.8 (5.8%)
Temp (°C)	5.4	5.1	−0.3 (−6.4%)	2.4	1.9	−0.5 (−21.9%)
Sea-ice con (-)	0.003	0.008	0.005 (163.7%)	0.063	0.112	0.049 (77.5%)
PAR (W m^{-2})	45.3	44.9	−0.5 (−1.0%)	38.2	35.7	−2.4 (−6.4%)
Nitr (μM)	3.1	3.4	0.3 (9.1%)	3.7	4.2	0.5 (12.9%)
Nitr$_{win}$ (μM)	11.3	11.3	0.07 (0.6%)	11.7	11.7	0.06 (0.5%)
MLD (m)	72.3	78.8	6.4 (8.9%)	73.7	68.9	−4.7 (−6.3%)
u^3 (m^{3}s$^{−3}$)	5.2e−7	4.7e−7	−5.0e−8 (−8.8%)	4.3e−7	3.7e−7	−6.0e−8 (−13.1%)
HT anom (TW)	2.8	−3.3	−6.1	2.8	−3.3	−6.1

Table 3. Statistics for multiple linear regression models of seasonal mean gross primary production (GPP) vs. temperature, wind-induced mixed layer turbulent energy production (u*^{3}) and light (PAR).

Independent var.	Dependent var.	Coeff.	Std.error	*t*-value	*p*-value
Barents Sea north ($R^2 = 0.62$)					
GPP (gC m^{-2} sn^{-1})	Temp (°C)	3.42e−01	9.69e−02	3.526	<0.001
	u*^{3} (m^{3}s^{-3})	3.27e−01	8.20e−02	3.984	0.0002
	PAR (W m^{-2})	4.38e−01	9.74e−02	4.501	0.00003
Barents Sea south ($R^2 = 0.34$)					
GPP (gC m^{-2} sn^{-1})	Temp (°C)	3.27e−01	1.19e−01	2.744	<0.01
	u*^{3} (m^{3}s^{-3})	4.15e−01	1.17e−01	3.555	<0.001
	PAR (W m^{-2})	3.67e−01	1.25e−01	2.934	<0.004

Individual regression beta-coefficients, standard errors as well as the associated *t*-values and *p*-values are listed.
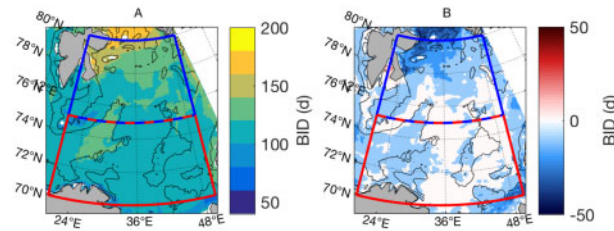
Figure 5. As in Figure 4, but for mean NORWECOM spring bloom initiation day (BID) (a) and corresponding change (b).

of the BS, particularly southeast of Svalbard (Figure 3b). The temperature is projected to rise by around 1°C in the northern region, and even more at some locations south and east of Svalbard. This pattern of BS warming, as well as the degree of warming, was similar to the CMIP3 A1B downscalings in Sandø et al. (2014b), and in particular the downscaled NCAR model therein. The reduction in sea-ice concentration in Figure 3d is also very similar to the downscaled NCAR model with the biggest losses in the northern parts of the BS between Svalbard and Frantz Josef Land. This area exhibited a decay in sea-ice concentrations between 2011 and 2014 (Ivanov et al., 2016), with broad,
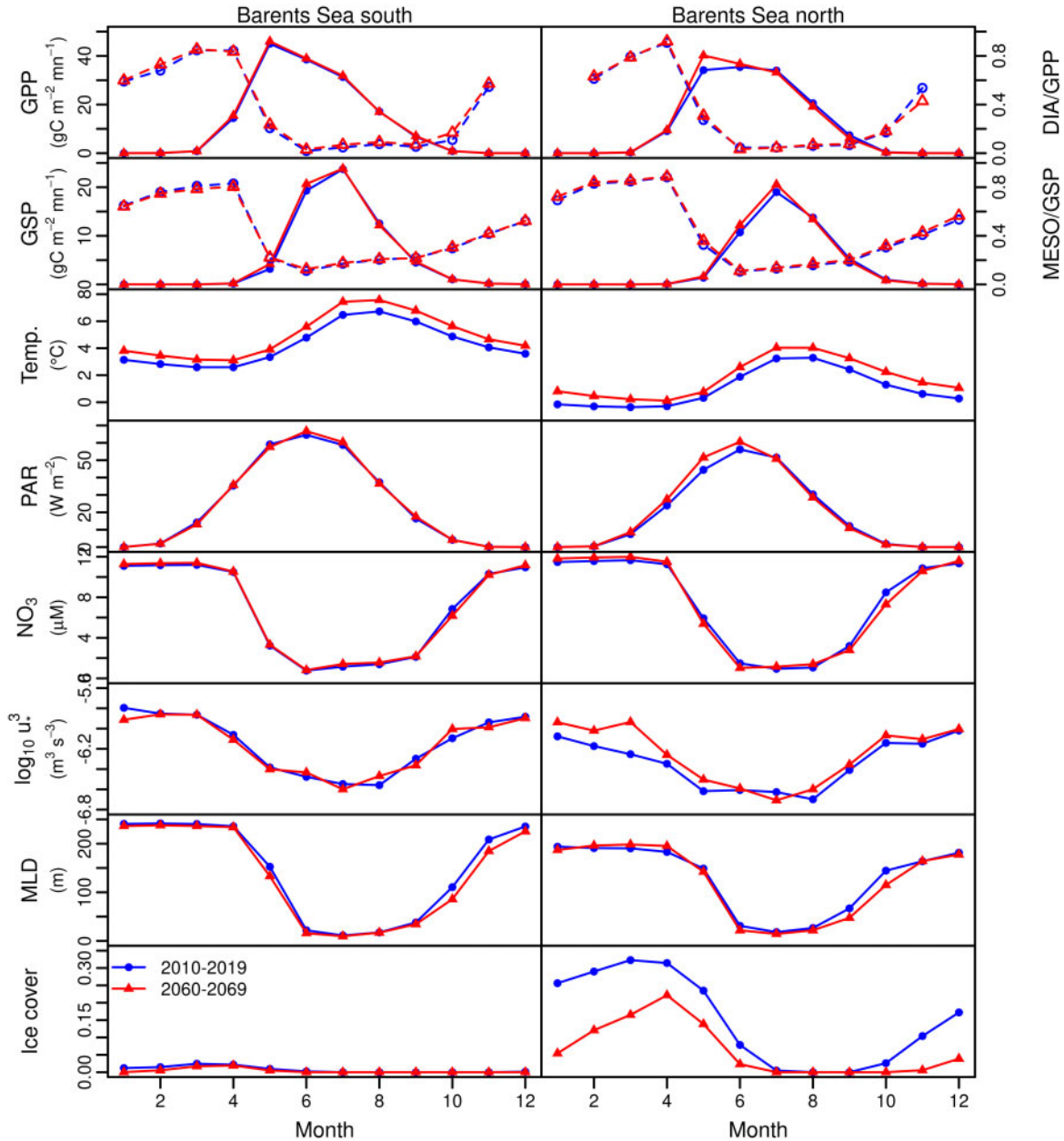
Figure 6. From upper to lower panel: Seasonal time series of gross primary production (GPP, left axis) and fraction of diatom gross production (DIA) vs. total GPP (dashed lines, right axis) in the present (blue) and future (red) decade in Barents Sea south (left panel) and north (right panel), gross secondary production (GSP, left axis) and fraction of meso-zooplankton gross production (MESO) vs. total GSP (dashed lines, right axis), temperature, light in terms of photosynthetic available radiance (PAR), production months nitrate concentration, wind-induced mixed layer turbulent energy production (u^{*3}), mixed layer depth (MLD), sea-ice concentration.
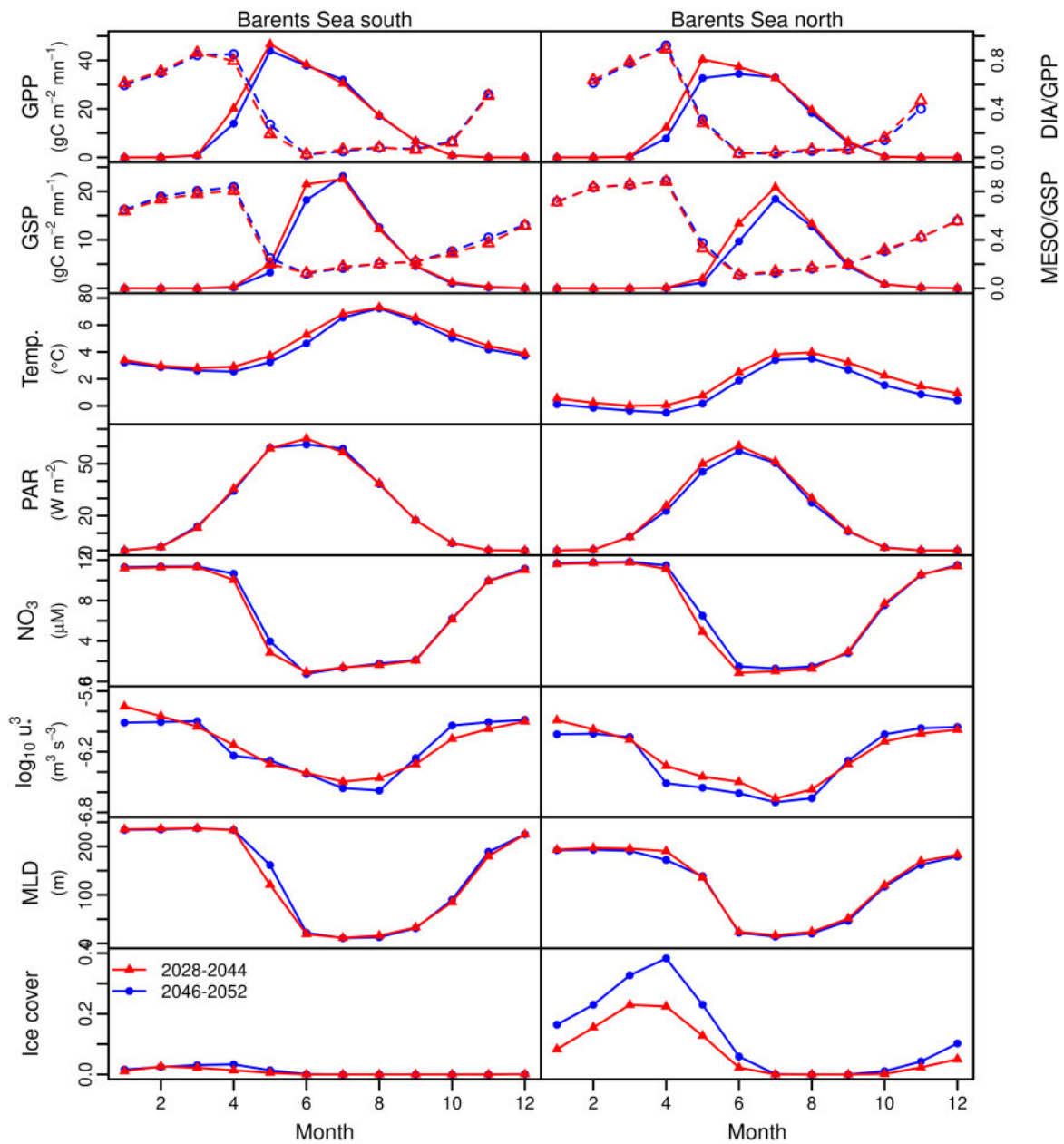
Figure 7. Same as in Figure 6, but for warm (2028–2044) and cold (2046–2052) periods.

long-living sea-ice-free areas in mid-winter (Onarheim *et al.*, 2014). Increased heat transports through the Fram Strait and BSO and subsequent bottom melting have been shown to be important for the sea-ice variability in the Arctic Ocean and BS, respectively (Sandø *et al.*, 2014a). The sea-ice decay north of Svalbard and in the northernmost parts of the BS is therefore probably related to increased seasonality of the Arctic sea-ice concentration, enabling increased influence of oceanic heat transported by the Atlantic Water at intermediate depths on the sea-ice above (Ivanov *et al.*, 2016). Increased heat transport through the BSO was also shown to have a strong influence on the sea-ice concentration in the BS in terms of reduced congelation growth and sea-ice formation (Sandø *et al.*, 2014a). This, in combination with less sea-ice import from the Arctic and corresponding loss in freshwater content and weakened ocean stratification (Lind *et al.*,

2018), have enhanced vertical mixing and increased upward fluxes of heat and salt that prevent sea-ice formation.

Figure 2 shows that GPP changes were found to largely follow changes in ocean temperature, sea-ice concentration, light, and wind-induced mixed layer turbulent energy production. However, the relative importance of the environmental variables differ in the southern and northern BS, and based on the regression coefficients in Table 3, it can be concluded that light (as a function of sea-ice extent) is most important for the GPP in the northern part while wind-induced turbulent energy production (and thus nutrient availability in the growth season) dominates in the southern part. Furthermore, wind-induced mixed layer turbulent energy production covaries with the heat transport in the BSO due to a common denominator; the atmospheric wind field which has been shown to push warm Atlantic Water through the

BSO (Ådlandsvik and Loeng, 1991; Ingvaldsen et al., 2004). In turn, both wind and heat transports affect the mixed layer depth in terms of density stratification and wind mixing. Many of the factors that are thought to be important for primary and secondary production are therefore themselves mutually dependent on each other. Dalpadado et al. (2014) found that increased open water area is the key driver of the changes in annual net primary production in the northern and eastern areas of the BS. The importance of simulating a realistic mixed layer depth outside sea-ice covered regions was studied by Lee et al. (2016), who assessed the net primary productivity and environmental variables from different regional and global biogeochemical models in the Greenland and Barents Seas. They found that the model skill of surface nitrate was best associated with how well the mixed layer depth was reproduced.

Table 1 shows that GPP increases slightly in both parts of the BS, which is different from the results of Slagstad et al. (2015) who showed a decrease of GPP in most of the BS. In our case, GPP is not limited by pre-bloom nitrate in any parts of the BS, which increases in parallel to increased temperature and inflow through the BSO. Ocean temperature may also have a direct effect on productivity, e.g., through changes in max growth rate, different effects on zooplankton and phytoplankton as well as increased turnover (Laufkötter et al., 2015; Nakamura and Oka, 2019), but this effect has not been included in the analysis here.

Decadal variability and abrupt changes

The RCP4.5 scenario leads to a general warming trend during the simulation time. However, the relatively large inter-annual to decadal variations in temperature cannot be explained by global warming and anthropogenic emissions alone as these are small, but positive every year. Also, light did not change significantly in the southern BS, suggesting that the local solar-induced warming was not an important factor controlling the general temperature trend there. The BS temperature is significantly affected by heat transported by ocean currents. One of the major heat inputs comes from the warm extension of the North Atlantic Current which flows along the Norwegian Coast and into the BS through the BSO as the Norwegian Atlantic Current. The heat transport anomaly showed a general increase, consistent with the increase in surface temperature in both regions (Figure 2). In addition, the heat transport showed large inter-annual to decadal variability. These variations were also consistent with the changes in temperature during the simulation period. Thus, from 2010 to the late 2020s, the heat transport decreased generally less than the overall trend. From the late 2020s until the beginning of the 2040s the heat transport is generally high, consistent with higher surface temperature, decreased sea-ice concentration, increased light availability, and high GPP and GSP. In the beginning of the 2040s, the heat transport decreased significantly, again consistent with patterns related to changes in temperature. Thus, shifts in the northern and southern BS in terms of both environment and productivity appear to be largely controlled by changes in the heat transport through the BSO. However, where the impact of heat transport in the north primarily worked through shifts in the sea-ice concentration and light availability, the impact in the south worked primarily to influence changes in mixed layer dynamics and nutrient availability in the spring bloom season.

Similar conclusions for the Bering Sea in the North Pacific were drawn by Banas et al. (2016). They used a planktonic ecosystem model for the Eastern Bering Sea to show that temperature and sea-ice concentration straightforwardly control the inter-annual to decadal variations in spring primary production. Further south, where the sea-ice extent is considerably less, the total primary production is increasingly controlled by nutrient supply, with both advective transport and turbulent mixing as contributors to inter-annual variability. In short, the relative importance of nutrient supply varies with latitude (Banas et al., 2016).

The temperature-dependent advance in timing of the spring bloom found here is supported by results of Lewandowska and Sommer (2010) who performed a mesocosm study where both the influence of light and temperature were taken into account. They also found that warming resulted in a shift towards smaller cell sizes which is potentially related to more nutrient-depleted conditions at the surface that favours small phytoplankton production at the expense of diatoms (Bopp et al., 2005). In this study, we did not observe a shift in size structure (from diatoms to flagellates) in the future despite a modest increase in temperature. However, while the temperature can have a direct effect on size composition (Mousing et al., 2014), the major effect of temperature is indirect through modulation of mixed layer dynamics and nutrient transport (Maranon et al., 2012). In this study, we found an increase in nitrate concentrations during the modelled period which was associated with changes in Atlantic Water inflow. Thus, the increase in nitrate has likely negated negative impacts of warming on nutrient availability during the spring bloom period.

In theory, an early spring bloom could lead to a mismatch between GPP and GSP, but the time series shown in Figures 6 and 7 do not show any indication of this as increases in GPP are followed by increases in GSP about 1 month later. Such a mismatch between the spring bloom and the dominant zooplankton was not found in the data collected around Svalbard in 2006, despite the fact that the retreat of sea-ice was particularly early this year (Norrbin et al., 2009).

Teasing out individual causal effects of the different variables is, however, not trivial as they, to a large degree, are dependent on each other. As discussed above, a dependency was clearest between temperature and sea-ice concentration where decreased heat input to the BS leads to increased sea-ice concentration and decreased access to light, especially in the northern region. Furthermore, warm periods usually coincide with shallow MLD. This is not the case in cold periods, especially not during the cold years 2046–2052 when MLD in the northern and southern BS are anti-correlated. The unusually shallow MLD in the north may then be related to relative strong stratification, caused and maintained by high sea-ice extent preventing high heat losses to the atmosphere and associated convection processes. Finally, the greatest effect of wind mixing and subsequent vertical mixing of nutrients was seen in the southern part of the BS. The mixed layer turbulence energy production shown in Figure 2 reflects a wind stress which on average is greater in the south compared to the north. The reason why there on average is more wind-induced mixed layer turbulence energy production in the southern part might be related to the fact that most cyclones in the BS generate over open water and lose energy over sea-ice as there is no energy to feed them (Madonna et al., 2020).

Implications for higher trophic levels

A frequently asked question in climate research as well as in research related to marine ecosystems is if the Arctic will become the new Atlantic (Fossheim *et al.*, 2015; Ivanov *et al.*, 2016; Polyakov *et al.*, 2017). Our results show a weak positive trend in GPP and GSP in the BS. Projections based on high emission scenarios also tend to show increased primary production in the Arctic due to decreased sea-ice concentration there (Yool *et al.*, 2015). Only the lower trophic levels (phyto- and zooplankton) were included in the ecosystem model in this study. However, as mentioned in the introduction, the temperature has direct and indirect effects on all trophic levels, from primary (Rose and Caron, 2007) and secondary production (Campbell *et al.*, 2001), to larval fish (Sundby, 2000) and mammals and seabirds (Hátún *et al.*, 2009, 2017). Plankton biomass production (GPP and GSP) forms the bottom of the food web, and changes here affect food availability to subsequent species higher in the trophic structure. In the southeastern BS, Dalpadado *et al.* (2014) found statistically significant linkages between net primary production and fish biomass, indicating bottom-up trophic interactions in this region. Recent observations and model simulations have shown that a warmer ocean and retreating sea-ice edge may have the potential to affect the population dynamics of keystone species of the sea-ice-associated food web, such as the polar cod (Boreogadus saida) (Huserbråten *et al.*, 2019). Likewise, the spawning sites of Northeast Arctic cod (Gadus morhua), which also grazes close to the sea-ice edge, may be shifted further northeastward with new locations at the Russian coast close to Murmansk in a warmer climate (Sandø *et al.*, 2020). From this point of view, we hypothesize that the results presented in this study can contribute to a better estimate of future changes in important fish stocks. Changes in GPP and GSP were found to sometimes be substantial between subsequent years and can to a large degree be coupled to changes in the physical environment. Årthun *et al.* (2018) found that the total stock biomass of Northeast Arctic Cod is predictable up to 7 years in advance based on hydrographic anomalies propagating from the North Atlantic to the BS. While we cannot directly quantify the effects on higher trophic levels, the literature supports that the factors presented here do indeed affect the biomass of economically important fish stocks such as the Northeast Arctic Cod (Sundby, 2000; Drinkwater *et al.*, 2010; Dalpadado *et al.*, 2012; Årthun *et al.*, 2018).

Summary and conclusions

An earth system model has here been downscaled for the RCP4.5 scenario for the period 2010–2070 and combined with a biophysical model to study how future variability and trends in temperature, sea-ice extent, light and wind-induced mixing in the BS affect the lower trophic levels in the marine ecosystem. The regional model was evaluated with respect to volume transports and sea-ice extent, which are both supposed to be important environmental variables for the plankton production in the BS. The model reproduced the mean values of the time series better than their variability, but the overall evaluation gave satisfactory results. The mean values of primary and secondary production from the ecosystem model were also found to be comparable with observational estimates from recent years, although somewhat higher.

In the future projection, both GPP and GSP were higher in the south compared to the north. There was a small increase and shift in the ratio between GSP and GPP, meaning a relative increase in zooplankton production compared to phytoplankton production. The small increase in GPP and GSP generally followed the small increase in nutrients over the period. Also, nitrate concentrations during the productive season were, like the pre-bloom concentrations, higher in the north compared to the south. Nutrients are therefore probably not a limiting factor in the northern BS. Instead, change in available light seems to be driving the relatively larger change in GPP there.

While GPP and GSP showed similar drops in the mid-2040s, the mechanisms differed between the regions. In the north, the drop in production was primarily caused by a drop in temperature which led to increases in sea-ice concentration and resulting in less light. That light is the primary limiting factor in the north is supported by the nitrate concentration during the production months, which is significantly higher in the north, and not decreasing in this period. In the south, the drop in GPP in the 2040s was partly caused by a drop in temperature which increased the mixed layer depth. With a concomitant decrease in mixing energy, less nutrients would be supplied towards the surface through mixing during the growth season. This is indirectly supported by the relatively low pre-bloom nitrate concentration.

In summary, general changes in GPP were significantly related to changes in the above-mentioned climate-related variables, with the highest GPP values being associated with warm periods, low sea-ice concentration, high PAR, and with a concomitant high wind-induced input of mixed layer turbulent energy and nutrients to the mixed layer. In contrast, low values of GPP, such as the large drop in the mid-2040s, were associated with low temperature, high sea-ice concentration, low PAR, and low input of mixed layer turbulent energy and nutrients.

While the results support that global warming, through changes in temperature, sea-ice concentration, and mixed layer depth appear to lead to an increase in both GPP and GSP in the BS, the effects of regionally or locally imposed changes in the environment such as inter-annual variations of volume and heat transport through the BSO and variable sea-ice extent are much more important. This conclusion highlights the importance of using downscaled ocean models to understand regional changes in ecosystem productivity and structure in response to climate change. However, it should be noted that the present study is only using one future scenario (RCP4.5) and one realization of it through the NorESM1-M climate model. This is a clear limitation and has to be taken into consideration when interpreting the results. The present projection should therefore only be considered as one member of a future ensemble of studies on the consequences of climate change.

A Ecosystem modeldescription

NORWECOM.E2E, a coupled physical, chemical, biological model system, was developed to study primary production, nutrient budgets and dispersion of particles such as fish larvae and pollution (Svendsen *et al.*, 1996; Skogen *et al.*, 1997; Søiland and Skogen, 2000; Skogen *et al.*, 2004; Skogen and Mathisen, 2009) and has also been extended with a module to project ocean acidification (Skogen *et al.*, 2014), and with Individual Based Models (IBMs) for *C. finmarchicus* (Hjøllo *et al.*, 2012) and pelagic fish (Utne *et al.*, 2012).

The biochemical model is coupled to the physical model through the light, the hydrography and the horizontal velocities and vertical mixing. The prognostic variables are dissolved inorganic nitrogen (NIT), phosphorous and silicate (SI), two different types of phytoplankton (diatoms and flagellates), two detritus (dead organic matter) pools (N and P), diatom skeletal (biogenic) silica, and oxygen (OXY). Two types of zooplankton (meso- and micro-zooplankton) are included based on a module taken from the ECOHAM4 model (Moll and Stegert, 2007; Pätsch *et al.*, 2009; Stegert *et al.*, 2009). The processes included are primary and secondary production, respiration, algae death, remineralization of inorganic nutrients from dead organic matter, self-shading, turbidity, sedimentation, resuspension, sedimental burial, and denitrification. The material produced by mortality is partly regenerated through the detritus pool, but a fraction of 10% is instantly regenerated as dissolved inorganic nitrogen (in nature as ammonia) and 25% as phosphorous available for uptake by phytoplankton (Bode *et al.*, 2004; Garber, 1984). Parameterization of the biochemical processes is taken from literature based on experiments in laboratories and mesocosms, or deduced from field measurements (Aksnes *et al.*, 1995; Pohlmann and Puls, 1994; Mayer, 1995; Gehlen *et al.*, 1995; Lohse *et al.*, 1995, 1996). A short overview of the biochemical model is given below. For more details, the reader should refer to Skogen *et al.* (1995), Skogen and Søiland (1998), and Pätsch *et al.* (2009). Some constants are given in Table 4.

A.1 Incident irradiation

The incident irradiation is modelled using a climatological light formulation (Skartveit and Olseth, 1986, 1987). The irradiance is split into a diffuse and a direct component:

$$H_x(h, n) = I_0(n) \cdot Tr_{0x}(n) \cdot F_x(h). \qquad (1)$$

Here, $H_x(h, n)$ is either direct ($x = \text{dir}$) or diffuse ($x = \text{dif}$) irradiance at the surface, $I_0(n)$ is the solar irradiance at normal incidence just outside the atmosphere, and $Tr_{0x}(n)$ is the transmittance at overhead zenith sun given by:

$$Tr_{0x}(n) = a_x(1 + b_x \cos \frac{n - c_x}{365} 2\pi). \qquad (2)$$

$F_x(h)$, the solar elevation function, is estimated in every internal time step, and given by:

$$F_x(h) = d_x + e_x \sin h - f_x (\sin h)^{1/2}, \qquad (3)$$

where h is the solar elevation and n the day number.

This model gives a climatological light formulation as a function of the area dependent constants $a_x - f_x$. An interpolation technique for these constants has been developed to include data for total daily irradiance, and the daily downward solar radiation flux has been used. The formula are valid when the solar elevation is above 5°, but they have been used for all solar elevations.

A.2 Light in the water column

Total light is the sum of direct and diffuse light. The diffuse light is calculated from

$$I_{\text{dif}}(x, y, z, t) = \text{PAR} \cdot R_{\text{dif}}(x, y, t) e^{-\frac{\kappa(x,y,z,t)}{\mu}}, \qquad (4)$$

where $R_{\text{dif}}(x, y, t) = H_{\text{dif}}(h, n)$, the diffuse component of the surface irradiance, and PAR, photosynthetic available radiance, a constant which converts from incident diffuse irradiation to photosynthetic available radiance. μ is the mean cosine of the diffuse light (Sathyendranath and Platt, 1990), and κ the attenuation coefficient:

$$\kappa = b_2 z + \frac{\nu}{\text{N2Chla}} \int_0^z (\text{DIA}(x, y, z, t) + \text{FLA}(x, y, z, t)) dz. \qquad (5)$$

Here, ν is the chlorophyll a light extinction coefficient, N2Chla the fraction of nitrate and chlorophyll_a in a cell, and b_2 extinction due to water and other substances.

A similar formulation is given for the direct light, $I_{\text{dir}}(x, y, z, t)$, by substituting R_{dif} with R_{dir} and μ with $\cos \phi$, where ϕ is the zenith angle of the direct light in the water column.

A.3 Phyto plankton production

The relationship between phytoplankton production and light intensity, and the relationship between phytoplankton production and nutrient uptake is represented by an affinity formulation, see

Table 4. NORWECOM.E2E constants.

Constant	Explanation	Value
a_1	Diatom production maximum at 0°C	1.53e−5 (s^{-1})
a_2	Diatom temperature dependent P_{max}	0.063 (°C^{-1})
a_3	Flagellate production maximum at 0°C	1.02e−5 (s^{-1})
a_4	Flagellate temperature dependent P_{max}	0.063 (°C^{-1})
a_5	Metabolic loss rate at 0°C	8.05e−7 (s^{-1})
a_6	Metabolic loss rate temp. dependence	0.07 (°C^{-1})
b_2	Extinction due to water and non-chlorophyll	0.07 (m^{-1})
μ	Mean cosine of diffuse light zenith angle	0.83
ν	Chl_a light extinction coefficient	1.38e−2 (m mg Chl_a^{-1})
N2CHLA	Cellular fraction of nitrate and Chl_a	11.0 (mg N mg Chl_a^{-1})
O2N	Fraction OXY/NIT for each cell produced	19.71 (mg O/mg N)
O2N$_{\text{denit}}$	Fraction OXY/NIT for the denitrification	3.42 (mg O/mg N)
PAR	Photosynthetic active irradiance	40%
T$_0$	Reference temperature	13°C

Aksnes *et al.* (1995). The combined effects of nutrient and light limitation are given by:

$$\mu_{\mathrm{dia}}(x, y, z, t) = \mu_{\max} \cdot N_{\lim} \cdot Dia(x, y, z, t), \quad N_{\lim} = \min_{1 \le i \le 4} V_i, \tag{6}$$

and

$$V_i = \frac{S_i}{S_i + \frac{\mu_{\max}(T)}{\alpha_i}}, \, i = 1, \ldots, 4 \tag{7}$$

is a modified Michaelis–Menten limitation for substance S_i. In the equations $i = 1$ corresponds to irradiance, $i = 2$ to nitrate, $i = 3$ to phosphate and $i = 4$ to silicate. In this formulation, the use of constant half saturation parameters, K_s, has been avoided. According to Aksnes and Egge (1991), they are made temperature dependent through the affinity parameter, α_i, defined as:

$$\alpha_i = \frac{\mu_{\max}(T_0)}{K_{S_i}}, \tag{8}$$

where K_{S_i} is the conventional half saturation constant at temperature T_0. $\mu_{\max}$ is the specific growth rate of the population under optimum light and nutrient conditions and made temperature dependent as suggested by Eppley (1972). The relation

$$\mu_{\max}(x, y, z, t) = a_1 e^{a_2 T(x,y,z,t)}, \tag{9}$$

has been chosen.

The metabolic losses are assumed to be related to the temperature according to the equation

$$R_{\mathrm{dia}}(x, y, z, t) = a_5 \mathrm{Dia}(x, y, z, t) e^{a_6 T(x,y,z,t)}, \tag{10}$$

and the death rate (in the whole water column) is assumed to be at a constant rate (1% day^{-1}) as long as the concentration of the algae somewhere in the column is above a minimum level. Below that level the death rate is zero, in order to prevent the algae in the model becoming extinct because of light limitation during winter. All these expressions refer to the diatoms. Analogous formulations are used for the production of flagellates. The only difference is that silicate is not rate-limiting for the flagellates. The biological parameter values were chosen according to independent validation against mesocosm experiments (Aksnes *et al.*, 1995).

A.4 Zoo plankton production

Secondary production is modified from the ECOHAM4 model (Moll and Stegert, 2007; Pätsch *et al.*, 2009; Stegert *et al.*, 2009). Zooplankton concentration is affected by feeding, excretion, faecal pellets production, and mortality.

Zooplankton concentration is given i nitrogen units (mgN m^{-3}). More detailed the change in the nitrogen component of mesozooplankton, *zen*, is given by:

$$\partial zen = p1n_{zen} + d1n_{zen} + zin_{zen} - zen_d 1n - zen_{don} - zen_n h4 + tra(zen), \tag{11}$$

where *p1n* is the first phytoplankton species (diatoms), *d1n* is

detritus, *zin* is microzooplankton, *don* is dissolved organic nitrogen, *nh4* is ammonium and *tra(zen)* represents transport (advection and diffusion) of mesozooplankton. Order of the components in each term represent the direction of the flux of matter from_to. For more details on each term please refer to Pätsch *et al.* (2009). A similar formulation can be given for microzooplankton, except that microzooplankton only feed on the second phytoplankton (flagellates) and detritus. For the feeding neither microzooplankton nor mesozooplankton has any food preference, thus the uptake is balanced proportional to the food concentrations.

A.5 Oxygen

The oxygen concentration is affected by the primary production, respiration, and re-mineralization of detrital matter. The amount of oxygen released by primary production is proportional to the amount of inorganic nitrogen consumed, and is given by constant, *O2N*. The same ratio for oxygen consumption is used for the respiration and re-mineralization process. The ratio is based on the assumption that inorganic nitrogen is converted from nitrate to organic matter and vice versa. For the fraction of nitrogen that is denitrified in the sediments, somewhat less consumption takes place.

Supplementary data

Supplementary material is available at the *ICESJMS* online version of the manuscript.

Data availability

The data underlying this article will be shared on reasonable request to the corresponding author.

References

Ådlandsvik, B. 2008. Marine downscaling of a future climate scenario for the North Sea. Tellus, 60A: 451–458.

Ådlandsvik, B., and Bentsen, M. 2007. Downscaling a twentieth century global climate simulation to the North Sea. Ocean Dynamics, 57: 453–466.

Ådlandsvik, B., and Loeng, H. 1991. A study of the climatic system in the Barents Sea. Polar Research, 10: 45–50.

Aksnes, D., and Egge, J. 1991. A theoretical model for nutrient uptake in phytoplankton. Marine Ecology Progress Series, 70: 65–72.

Aksnes, D., Ulvestad, K., Baliño, B., Berntsen, J., Egge, J., and Svendsen, E. 1995. Ecological modelling in coastal waters: towards predictive physical-chemical-biological simulation models. Ophelia, 41: 5–36.

Arrigo, K. R., van Dijken, G., and Pabi, S. 2008. Impact of a shrinking Arctic ice cover on marine primary production. Geophysical Research Letters, 35: 1–6.

Årthun, M., Bogstad, B., Daewel, U., Keenlyside, N. S., Sandø, A. B., Schrum, C., and Ottersen, G. 2018. Climate based multi-year predictions of the Barents Sea cod stock. PLoS One, 13: e0206319.

Årthun, M., Eldevik, T., Smedsrud, L. H., Skagseth, Ø., and Ingvaldsen, R. 2012. Quantifying the influence of Atlantic heat on

Barents Sea ice variability and retreat. Journal of Climate, 25: 4736–4743.

Banas, N. S., Zhang, J., Campbell, R. G., Sambrotto, R. N., Lomas, M. W., Sherr, E., Sherr, B., et al. 2016. Spring plankton dynamics in the eastern Bering Sea, 1971–2050: mechanisms of interannual variability diagnosed with a numerical model. Journal of Geophysical Research: Oceans, 121: 1476–1501.

Barton, A. D., Irwin, A. J., Finkel, Z. V., and Stock, C. A. 2016. Anthropogenic climate change drives shift and shuffle in North Atlantic phytoplankton communities. Proceedings of the National Academy of Sciences United States of America, 113: 2964–2969.

Behrenfeld, M. J., O'Malley, R. T., Siegel, D. A., McClain, C. R., Sarmiento, J. L., Feldman, G. C., Milligan, A. J., et al. 2006. Climate-driven trends in contemporary ocean productivity. Nature, 444: 752–755.

Bentsen, M., Bethke, I., Debernard, J. B., Iversen, T., Kirkevåg, A., Seland, Ø., Drange, H., et al. 2013. The Norwegian Earth System Model, NorESM1-M Part 1: description and basic evaluation of the physical climate. Geoscientific Model Development, 6: 687–720.

Bode, A., Barquero, S., Gonzales, N., Alvarez-Ossorio, M., and Varela, M. 2004. Contribution of heterotrophic plankton to nitrogen regeneration in the upwelling ecosystem of La Coruna (NW Spain.). Journal of Plankton Research, 26: 11–28.

Böning, C. W., Dispert, A., Visbeck, M., Rintoul, S. R., and Schwarzkopf, F. U. 2008. The response of the Antarctic Circumpolar Current to recent climate change. Nature Geoscience, 1: 864–869.

Bopp, L., Aumont, O., Cadule, P., Alvain, S., and Gehlen, M. 2005. Response of diatoms distribution to global warming and potential implications: a global model study. Geophysical Research Letters, 32: 1–4.

Bopp, L., Resplandy, L., Orr, J. C., Doney, S. C., Dunne, J. P., Gehlen, M., Halloran, P., et al. 2013. Multiple stressors of ocean ecosystems in the 21st century: projections with CMIP5 models. Biogeosciences, 10: 6225–6245.

Box, G. E., Jenkins, G. M., Reinsel, G. C., and Ljung, G. M. 2015. Time Series Analysis: Forecasting and Control. Wiley, Hoboken, New Jersey, USA.

Brody, S. R., Lozier, M. S., and Dunne, J. P. 2013. A comparison of methods to determine phytoplankton bloom initiation. Journal of Geophysical Research: Oceans, 118: 2345–2357.

Brown, J. H., Gillooly, J. F., Allen, A. P., Savage, V. M., and West, G. B. 2004. Toward a metabolic theory of ecology. Ecology, 85: 1771–1789.

Budgell, W. P. 2005. Numerical simulation of ice-ocean variability in the Barents Sea region towards dynamical downscaling. Ocean Dynamics, 55: 370–387.

Burnham, K., and Anderson, D. 2002. Model Selection and Multimodel Inference. A Practical Information-Theoretic Approach. Springer, New York.

Campbell, R. G., Wagner, M. M., Teegarden, G. J., Boudreau, C. A., and Durbin, E. G. 2001. Growth and development rates of the copepod Calanus finmarchicus reared in the laboratory. Marine Ecology Progress Series, 221: 161– 183.

Cheng, L., Trenberth, K. E., Fasullo, J., Boyer, T., Abraham, J., and Zhu, J. 2017. Improved estimates of ocean heat content from 1960 to 2015. Science Advances, 3: e1601545.

Dalpadado, P., Arrigo, K. R., Hjøllo, S. S., Rey, F., Ingvaldsen, R. B., Sperfeld, E., van Dijken, G. L., et al. 2014. Productivity in the Barents Sea - response to recent climate variability. PLoS One, 9: e95273.

Dalpadado, P., Ingvaldsen, R. B., Stige, L. C., Bogstad, B., Knutsen, T., Ottersen, G., and Ellertsen, B. 2012. Climate effects on Barents Sea ecosystem dynamics. ICES Journal of Marine Science, 69: 1–14.

Drinkwater, K., Beaugrand, G., Kaeriyama, M., Kim, S., Ottersen, G., Perry, R. I., Portner, H.-O., et al. 2010. On the processes linking climate to ecosystem changes. Journal of Marine Systems, 79: 374–388.

Eppley, R. W. 1972. Temperature and phytoplankton growth in the sea. Fishery Bulletin, 70: 1063–1085.

Fossheim, M., Primicerio, R., Johannesen, E., Ingvaldsen, R. B., Aschan, M. M., and Dolgov, A. V. 2015. Recent warming leads to a rapid borealization of fish communities in the Arctic. Nature Climate Change, 5: 673–677.

Frölicher, T. L., Rodgers, K. B., Stock, C. A., and Cheung, W. W. L. 2016. Sources of uncertainties in 21st century projections of potential ocean ecosystem stressors. Global Biogeochemical Cycles, 30: 1224–1243.

Garber, J. 1984. Laboratory study of nitrogen and phosphorous remineralization during decomposition of coastal plankton and seston. Estuarine, Coastal and Shelf Science, 16: 685–702.

Gehlen, M., Malschaert, H., and Raaphorst, W. 1995. Spatial and temporal variability of benthic silica fluxes in the southeastern North Sea. Continental Shelf Research, 13: 1675–1696.

Hansen, J., Sato, M., Ruedy, R., Lo, K., Lea, D. W., and Medina-Elizade, M. 2006. Global temperature change. Proceedings of the National Academy of Sciences of the United States of America, 103: 14288–14293.

Hátún, H., Payne, M. R., Beaugrand, G., Reid, P. C., Sandø, A. B., Drange, H., Hansen, B., et al. 2009. Large bio-geographical shifts in the northeastern Atlantic - from the subpolar gyre, via plankton and blue whiting, to pilot whales. Progress in Oceanography, 80: 149–162.

Hawkins, E., and Sutton, R. 2009. The potential to narrow uncertainty in regional climate predictions. Bulletin of the American Meteorological Society, 90: 1095–1108.

Hermans, T. H. J., Tinker, J., Palmer, M. D., Katsman, C. A., Vermeersen, B. L. A., and Slangen, A. B. A. 2020. Improving sea-level projections on the Northwestern European shelf using dynamical downscaling. Climate Dynamics, 54: 1987–2011.

Hjøllo, S., Huse, G., Skogen, M. D., and Melle, W. 2012. Modelling secondary production in the Norwegian Sea with a fully coupled physical/primary production/individual- based Calanus finmarchicus model system. Marine Biology Research, 8: 508–526.

Hoegh-Guldberg, O., and Bruno, J. F. 2010. The impact of climate change on the world's marine ecosystems. Science, 328: 1523–1528.

Huserbråten, M., Eriksen, E., Gjøsæter, H., and Vikebø, F. 2019. Polar cod in jeopardy under the retreating Arctic sea ice. Communications Biology, 407: 1–8.

Hátún, H., Olsen, B., and Pacariz, S. 2017. The dynamics of the north Atlantic subpolar gyre introduces predictability to the breeding success of kittiwakes. Frontiers in Marine Science, 4: 123.

Ingvaldsen, R. B., Asplin, L., and Loeng, H. 2004. The seasonal cycle in the Atlantic transport to the Barents Sea during the years 1997–2001. Continental Shelf Research, 24: 1015–1032.

IPCC 2007. Climate Change 2007: The Physical Science Basis. Contribution of Working Group I to the Fourth Assessment Report of the Intergovernmental Panel on Climate Change. Cambridge University Press, Cambridge, United Kingdom and New York, NY, USA.

IPCC 2013. Climate Change 2013: The Physical Science Basis. Contribution of Working Group I to the Fifth Assessment Report of the Intergovernmental Panel on Climate Change. Cambridge University Press, Cambridge, United Kingdom and New York, NY, USA. 1535 pp.

Ivanov, V., Alexeev, V., Koldunov, N. V., Repina, I., Sandø, A. B., Smedsrud, L. H., and Smirnov, A. 2016. Arctic Ocean heat impact on regional ice decay: a suggested positive feedback. Journal of Physical Oceanography, 46: 1437–1456.

Jensen, L. Ø., Mousing, E. A., and Richardson, K. 2017. Using species distribution modelling to predict future distributions of phytoplankton: case study using species important for the biological pump. Marine Ecology, 38: e12427.

Johannesen, E., Ingvaldsen, R. B., Bogstad, B., Dalpadado, P., Eriksen, E., Gjøsæter, H., Knutsen, T., et al. 2012. Changes in Barents Sea ecosystem state, 1970–2009: climate fluctuations, human impact, and trophic interactions. ICES Journal of Marine Science, 69: 880–889.

Kahru, M., Brotas, V., Manzano-Sarabia, M., and Mitchell, B. G. 2011. Are phytoplankton blooms occurring earlier in the Arctic? Global Change Biology, 17: 1733–1739.

Klinger, B. A., Huang, B., Kirtman, B., Schopf, P., and Wang, J. 2006. Monthly climatologies of oceanic friction velocity cubed. Journal of Climate, 19: 5700–5708.

Knutson, T. R., Sirutis, J. J., Zhao, M., Tuleya, R. E., Bender, M., Vecchi, G. A., Villarini, G., et al. 2015. Global projections of intense tropical cyclone activity for the late twenty-first century from dynamical downscaling of CMIP5/RCP4.5 scenarios. Journal of Climate, 28: 7203–7224.

Large, W. G., and Yeager, S. G. 2009. The global climatology of an interannually varying air–sea flux data set. Climate Dynamics, 33: 341–364.

Laufkötter, C., Vogt, M., Gruber, N., Aita-Noguchi, M., Aumont, O., Bopp, L., Buitenhuis, E., et al. 2015. Drivers and uncertainties of future global marine primary production in marine ecosystem models. Biogeosciences, 12: 6955–6984.

Lee, Y. J., Matrai, P. A., Friedrichs, M. A. M., Saba, V. S., Aumont, O., Babin, M., Buitenhuis, E. T., et al. 2016. Net primary productivity estimates and environmental variables in the Arctic Ocean: an assessment of coupled physical-biogeochemical models. Journal of Geophysical Research: Oceans, 121: 8635–8669.

Lewandowska, A., and Sommer, U. 2010. Climate change and the spring bloom: a mesocosm study on the influence of light and temperature on phytoplankton and mesozooplankton. Marine Ecology Progress Series, 405: 101–111.

Lien, V. S., Gusdal, Y., Albretsen, J., Melsom, A., and Vikebø, F. 2013. Evaluation of a Nordic Seas 4 km numerical ocean model hindcast archive (SVIM), 1960-2011. Fisken og Havet, 7: Nordnesgt. 33, N-5005 Bergen, Norway.

Lien, V. S., Gusdal, Y., and Vikebø, F. B. 2014. Along-shelf hydrographic anomalies in the Nordic Seas (1960–2011). Locally generated or advective signals? Ocean Dynamics, 64: 1047–1059.

Lien, V. S., Hjøllo, S. S., Skogen, M. D., Svendsen, E., Wehde, H., Bertino, L., Counillon, F., et al. 2016. An assessment of the added value from data assimilation on modelled Nordic seas hydrography and ocean transports. Ocean Modelling, 99: 43– 59.

Lien, V. S., and Ådlandsvik, B. 2014. Bottom water formation as a primer for spring-blooms on Spitsbergenbanken? Journal of Marine Systems, 130: 241– 247.

Lind, S., Ingvaldsen, R. B., and Furevik, T. 2018. Arctic warming hotspot in the northern Barents Sea linked to declining sea-ice import. Nature Climate Change, 8: 634–639.

Liu, W., Xie, S.-P., Liu, Z., and Zhu, J. 2017. Overlooked possibility of a collapsed Atlantic Meridional overturning circulation in warming climate. Science Advances, 3: e1601666.

Lohse, L., Kloosterhuis, H. T., van Raaphorst, W., and Helder, W. 1996. Denitrification rates as measured by the isotope pairing method and by the acetylene inhibition technique in continental shelf sediments of the North Sea. Marine Ecology Progress Series, 132: 169–179.

Lohse, L., Malschaert, F., Slomp, C., Helder, W., and Raaphorst, W. 1995. Sediment-water fluxes of inorganic nitrogen compounds along the transport route of organic matter in the North Sea. Ophelia, 41: 173–197.

Lu, P., Li, Z., Cheng, B., and Leppäranta, M. 2011. A parameterization of the ice-ocean drag coefficient. Journal of Geophysical

Research: Oceans, 116: URL https://agupubs.onlinelibrary.wiley.com/doi/abs/10.1029/2010JC006878.

Madonna, E., Hes, G., Li, C., Michel, C., and Siew, P. Y. F. 2020. Control of Barents Sea wintertime cyclone variability by large--scale atmospheric flow. Geophysical Research Letters, 47.

Maranon, E., Cermeño, P., Latasa, M., and Tadonleke, R. 2012. Temperature, resources, and phytoplankton size structure in the ocean. Limnology and Oceanography, 57: 1266–1278.

Martinsen, E., and Engedahl, H. 1987. Implementation and testing of a lateral boundary scheme as an open boundary condition in a barotropic ocean model. Coastal Engineering, 11: 603–627.

Mayer, B. 1995. Ein dreidimensionales, numerisches schwebstoff--transportmodell mit anwendung auf die Deutsche Bucht. Tech. Rep. GKSS 95/E/59, GKSS-Forschungszentrum Geesthacht GmbH. ISSN 0344-9629, 104 pp.

Moll, A., and Stegert, C. 2007. Modeling Pseudocalanus elongatus population dynamics embedded in a water column ecosystem model for the northern North Sea. Journal of Marine Systems, 64: 35–46.

Mousing, E. A., Ellegaard, M., and Richardson, K. 2014. Global patterns in phytoplankton community size structure—evidence for a direct temperature effect. Marine Ecology Progress Series, 497: 25–38.

Nakamura, Y., and Oka, A. 2019. CMIP5 model analysis of future changes in ocean net primary production focusing on differences among individual oceans and models. Journal of Oceanography, 75: 441–462.

Norrbin, F., Eilertsen, H. C., and Degerlund, M. 2009. Vertical distribution of primary producers and zooplankton grazers during different phases of the Arctic spring bloom. Deep Sea Research Part II: Topical Studies in Oceanography, 56: 1945– 1958.

Onarheim, I. H., Eldevik, T., Årthun, M., Ingvaldsen, R. B., and Smedsrud, L. H. 2015. Skillful prediction of Barents Sea ice cover. Geophysical Research Letters, 42: 5364–5371.

Onarheim, I. H., Smedsrud, L. H., Ingvaldsen, R. B., and Nilsen, F. 2014. Loss of sea ice during winter north of Svalbard. Tellus A: Dynamic Meteorology and Oceanography, 66: 23933.

Orr, J. C., Fabry, V. J., Aumont, O., Bopp, L., Doney, S. C., Feely, R. A., Gnanadesikan, A., et al. 2005. Anthropogenic ocean acidification over the twenty-first century and its impact on calcifying organisms. Nature, 437: 681–686.

Pätsch, J., Kühn, W., and Moll, A. and H., L. 2009. ECOHAM4 user guide - ECOsystem model, HAMburg, version 4. Tech. Rep. 01-2009, Institut für Meereskunde, Hamburg, Germany.

Perry, A. L., Low, P. J., Ellis, J. R., and Reynolds, J. D. 2005. Climate change and distribution shifts in marine fishes. Science, 308: 1912–1915.

Pohlmann, T., and Puls, W. 1994. Currents and transport in water. In Circulation and Contaminant Fluxes in the North Sea, pp. 345–402. Ed. by J. Sündermann. Springer, Berlin.

Polyakov, I. V., Bekryaev, R. V., Alekseev, G. V., Bhatt, U. S., Colony, R. L., Johnson, M. A., Maskshtas, A. P., et al. 2003. Variability and trends of air temperature and pressure in the maritime Arctic, 1875–2000. Journal of Climate, 16: 2067–2077.

Polyakov, I. V., Pnyushkov, A. V., Alkire, M. B., Ashik, I. M., Baumann, T. M., Carmack, E. C., Goszczko, I., et al. 2017. Greater role for Atlantic inflows on sea-ice loss in the Eurasian Basin of the Arctic Ocean. Science, 356: 285–291.

Popova, E. E., Yool, A., Coward, A. C., Dupont, F., Deal, C., Elliott, S., Hunke, E., et al. 2012. What controls primary production in the Arctic Ocean? Results from an intercomparison of five general circulation models with biogeochemistry. Journal of Geophysical Research: Oceans, 117: n/a.

R Core Team 2019. R: A Language and Environment for Statistical Computing. R Foundation for Statistical Computing, Vienna, Austria.

Rahmstorf, S., Cazenave, A., Church, J. A., Hansen, J. E., Keeling, R. F., Parker, D. E., and Somerville, R. C. J. 2007. Recent climate observations compared to projections. Science, 316: 709–709.

Rose, J. M., and Caron, D. A. 2007. Does low temperature constrain the growth rates of heterotrophic protists? Evidence and implications for algal blooms in cold waters. Limnology and Oceanography, 52: 886–895.

Sandø, A. B., Gao, Y., and Langehaug, H. 2014a. Relation between ocean heat transports, sea ice processes and Arctic sea ice variability in NorESM1-M simulations. Journal of Geophysical Research, 119: 2095–2108.

Sandø, A. B., Johansen, G. O., Aglen, A., Stiansen, J. E., and Renner, A. H. H. 2020. Climate change and new potential spawning sites for Northeast Arctic cod. Frontiers in Marine Science, 7: 28.

Sandø, A. B., Melsom, A., and Budgell, W. P. 2014b. Downscaling IPCC control run and future scenario with focus on the Barents Sea. Ocean Dynamics, 64: 927–949.

Sandø, A. B., Nilsen, J. E. Ø., Gao, Y., and Lohmann, K. 2010. The importance of heat transports and local air-sea heat fluxes for the Barents Sea climate variability. Journal of Geophysical Research, 115: 1–11.

Sathyendranath, S., and Platt, T. 1990. The light field in the ocean: its modification and exploitation by the Pelagi Biota. *In* Light and Life in the Sea, pp. 333–344. Ed. by P. J. Herring. Cambridge, Cambridge University Press.

Schrum, C., Lowe, J., and Meier, M. 2015. Projected change - North Sea, . In North Sea Region Climate Change Assessment. Regional Climate Studies, edited by Quante M. and Colijn F, Springer, Cham.

Screen, J. A., and Williamson, D. 2017. Ice-free Arctic at 1.5°C? Nature Climate Change, 7: 230–231.

Shchepetkin, A. F., and McWilliams, J. C. 2005. The regional oceanic modeling system (ROMS): a split-explicit, free-surface, topography-following-coordinate oceanic model. Ocean Modelling, 9: 347–404.

Shchepetkin, A. F., and McWilliams, J. C. 2008. Quasi-monotone advection schemes based on explicit locally adaptive dissipation. Monthly Weather Review, 126: 1541–1580.

Skagseth, Ø., Slotte, A., Stenevik, E. K., and Nash, R. D. M. 2015. Characteristics of the Norwegian Coastal Current during years with high recruitment of Norwegian Spring Spawning Herring (*Clupea harengus* L.). PLoS One, 10: e0144117.

Skaret, G., Dalpadado, P., Hjøllo, S., Skogen, M., and Strand, E. 2014. *Calanus finmarchicus* abundance, production and population dynamics in the Barents Sea in a future climate. Progress in Oceanography, 125: 26–39.

Skartveit, A., and Olseth, J. A. 1986. Modelling slope irradiance at high lattitudes. Solar Energy, 36: 333–344.

Skartveit, A., and Olseth, J. A. 1987. A model for the diffuse fraction of hourly global radiation. Solar Energy, 37: 271–274.

Skogen, M., Budgell, W., and Rey, F. 2007. Interannual variability in Nordic Seas primary production. ICES Journal of Marine Science, 64: 889–898.

Skogen, M., and Mathisen, L. 2009. Long term effects of reduced nutrient inputs to the North Sea. Estuarine Coastal and Shelf Science, 82: 433–442.

Skogen, M., Olsen, A., Børsheim, K., Sandø, A., and Skjelvan, I. 2014. Modelling ocean acidification in the Nordic and Barents seas in present and future climate. Journal of Marine Systems, 131: 10–20.

Skogen, M., and Søiland, H. 1998. A User's Guide to NORWECOM v2.0. The NORWegian ECOlogical Model system. Tech. Rep. Fisken og Havet 18/98, Institute of Marine Research, Pb.1870, NO-5024 Bergen. 42 pp.

Skogen, M., Søiland, H., and Svendsen, E. 2004. Effects of changing nutrient loads to the North Sea. Journal of Marine Systems, 46: 23–38.

Skogen, M., Svendsen, E., Berntsen, J., Aksnes, D., and Ulvestad, K. 1995. Modelling the primary production in the North Sea using a coupled 3 dimensional Physical Chemical Biological Ocean model. Estuarine, Coastal and Shelf Science, 41: 545–565.

Skogen, M., Svendsen, E., and Ostrowski, M. 1997. Quantifying volume transports during SKAGEX with the Norwegian Ecological Model system. Continental Shelf Research, 17: 1817–1837.

Skogen, M. D., Hjøllo, S. S., Sandø, A. B., and Tjiputra, J. 2018. Future ecosystem changes in the Northeast Atlantic: a comparison between a global and a regional model system. ICES Journal of Marine Science, 75: 2355–2369.

Slagstad, D., Ellingsen, I., and Wassmann, P. 2011. Evaluating primary and secondary production in an Arctic Ocean void of summer sea ice: an experimental simulation approach. Progress in Oceanography, 90: 117–131.

Slagstad, D., Wassmann, P. F. J., and Ellingsen, I. 2015. Physical constrains and productivity in the future Arctic Ocean. Frontiers in Marine Science, 2: 85.

Smagorinsky, J. 1963. General circulation experiments with the primitive equations. Monthly Weather Review, 91: 99–164.

Søiland, H., and Skogen, M. 2000. Validation of a 3-D biophysical model using nutrient observations in the North Sea. ICES Journal of Marine Science, 57: 816–823.

Song, Y., and Haidvogel, D. 1994. A semi-implicit ocean circulation model using a generalized topography-following coordinate system. Journal of Computational Physics, 115: 228–244.

Stegert, C., Moll, A., and Kreus, M. 2009. Validation of the three-dimensional ECOHAM model in the German Bight for 2004 including population dynamics of *Pseudocalnus elongatus*. Journal of Sea Research, 62: 1–15.

Stroeve, J. C., Kattsov, V., Barrett, A., Serreze, M., Pavlova, T., Holland, M., Meier, W. N., *et al.* 2012. Trends in Arctic sea ice extent from CMIP5, CMIP3 and observations. Geophysical Research Letters, 39: 1–7.

Sundby, S. 2000. Recruitment of Atlantic cod stocks in relation to temperature and advection of copepod populations. Sarsia, 85: 277–298.

Svendsen, E., Bemtsen, J., Skogen, M., Ådlandsvik, B., and Martinsen, E. 1996. Model simulation of the Skagerrak circulation and hydrography during SKAGEX. Journal of Marine Systems, 8: 219–236.

Titov, O., and Orlova, E. 2011. Lower trophic levels. *In* The Barents Sea. Ecosystem, Resources and Management. Half a Century of Russian-Norwegian Cooperation, pp. 77–119. Ed. by T. Jakobsen and V. Ozhigin. Tapir Academic Press, Trondheim, Norway. 825 pp.

Utne, K., Hjøllo, S., Huse, G., and Skogen, M. 2012. Estimating consumption of Calanus finmarchicus by planktivorous fish in the Norwegian Sea using a fully coupled 3d model system. Marine Biology Research, 8: 527–547.

Vancoppenolle, M., Meiners, K. M., Michel, C., Bopp, L., Brabant, F., Carnat, G., Delille, B., *et al.* 2013. Role of sea ice in global biogeochemical cycles: emerging views and challenges. Quaternary Science Reviews, 79: 207–230.

Wassmann, P., Ratkova, T., Andreassen, I., Vernet, M., Pedersen, G., and Rey, F. 1999. Spring bloom development in the marginal ice zone and the Central Barents Sea. Marine Ecology, 20: 321–346.

Yool, A., Popova, E. E., and Coward, A. C. 2015. Future change in ocean productivity: is the Arctic the new Atlantic? Journal of Geophysical Research: Oceans, 120: 7771–7790.

Zhang, R., Delworth, T. L., and Held, I. M. 2007. Can the Atlantic Ocean drive the observed multidecadal variability in northern hemisphere mean temperature? Geophysical Research Letters, 34: 1–6: https://agupubs.onlinelibrary.wiley.com/doi/abs/10.1029/2006GL028683 (accessed 18 May 2021).

Handling editor: Mary Hunsicker